

Adiabatic association of ultracold molecules via magnetic field tunable interactions

Krzysztof Góral* and Thorsten Köhler

Clarendon Laboratory, Department of Physics, University of Oxford, Parks Road, Oxford, OX1 3PU, United Kingdom

Simon A. Gardiner

JILA, University of Colorado and National Institute of Standards and Technology, Boulder, Colorado 80309-0440

Eite Tiesinga and Paul S. Julienne

*Atomic Physics Division, National Institute of Standards and Technology,
100 Bureau Drive Stop 8423, Gaithersburg, Maryland 20899-8423*

(Dated: January 28, 2020)

We consider in detail the situation of applying a time dependent external magnetic field to a ^{87}Rb atomic Bose-Einstein condensate held in a harmonic trap, in order to adiabatically sweep the interatomic interactions across a Feshbach resonance to produce diatomic molecules. To this end, we introduce a minimal two-body Hamiltonian depending on just five measurable parameters of a Feshbach resonance, which accurately determines all low energy binary scattering observables, in particular, the molecular conversion efficiency of just two atoms. Based on this description of the microscopic collision phenomena, we use the many-body theory of T. Köhler and K. Burnett [Phys. Rev. A **65**, 033601 (2002)] to study the efficiency of the association of molecules in a ^{87}Rb Bose-Einstein condensate during a linear passage of the magnetic field strength across the 100 mT Feshbach resonance. We explore different, experimentally accessible, parameter regimes, and compare the predictions of Landau-Zener, configuration interaction, and two level mean field calculations with those of the microscopic many-body approach. Our comparative studies reveal a remarkable insensitivity of the molecular conversion efficiency with respect to both the details of the microscopic binary collision physics and the coherent nature of the Bose-Einstein condensed gas, provided that the magnetic field strength is varied linearly. We provide the reasons for this universality of the molecular production achieved by *linear* ramps of the magnetic field strength, and identify the Landau-Zener coefficient determined by F.H. Mies *et al.* [Phys. Rev. A **61**, 022721 (2000)] as the main parameter that controls the efficiency.

PACS numbers: 03.75.Kk, 34.50.-s, 05.30.-d

I. INTRODUCTION

The prospect of achieving quantum degenerate molecular gases has attracted considerable attention for some time now [1]. Such an accomplishment may open new avenues for research, for instance, bright sources of molecules for cold collision studies [2], precise molecular spectroscopy, elucidating the nature of a possible BCS-BEC crossover in Fermi gases [3] and, possibly, the exploitation of dipole-dipole interactions [4]. It has been clear from the outset, however, that laser cooling techniques, essential for the production of Bose-Einstein condensates and degenerate Fermi gases of atoms, are difficult to apply in the case of molecules due to their typically complicated rovibrational energy spectrum. The association of ultracold atoms into diatomic molecules, which may also be quantum degenerate, therefore seems a very promising route. The molecular conversion can be achieved by photoassociation [5] or by application of time dependent magnetic fields in the vicinity of Feshbach resonances [6]. The Feshbach resonance technique has recently been exploited with great success to produce large, ultracold assemblies of diatomic molecules, using as a source both atomic Bose-Einstein condensates [7, 8, 9, 10, 11] and

quantum degenerate two component gases of Fermionic atoms [12, 13, 14, 15, 16, 17, 18, 19, 20, 21, 22, 23].

The experiments reported in Refs. [9, 10, 11] achieve conversion of alkali atoms in dilute Bose-Einstein condensates to diatomic molecules by an adiabatic sweep of the strength of a homogeneous magnetic field across a Feshbach resonance from negative to positive scattering lengths. The observations indicate molecular fractions much smaller than the ideal limit of half the number of initial condensate atoms, even in the limit of perfect adiabaticity. This may be due to limitations in the initial production of molecules, or their long term stability in the presence of the surrounding gas.

The long term stability of the highest excited vibrational molecular bound state, produced by the adiabatic association technique, may be limited due to collisional deexcitation. Both theoretically and experimentally, very little is known about the associated rate constants for highly excited diatomic molecules composed of alkali atoms. To our knowledge, the only available exact calculations have been performed for the deexcitation of tightly bound Na_2 molecules upon collision with a Na atom [24]. From an experimental viewpoint, the comparatively high relative momenta of the products of collisional deexcitation have so far prevented their detection. Conclusive experimental studies of the loss rates and the underlying microscopic processes are therefore difficult to achieve.

In such an uncertain situation it is important to first understand the production of the diatomic molecules. In this paper we consider the situation of adiabatically sweeping the

*also at Center for Theoretical Physics, Polish Academy of Sciences, Al. Lotników 32/46, 02-668 Warsaw, Poland

magnetic field strength across a Feshbach resonance to form molecules from an initially Bose-Einstein condensed dilute gas of atoms. The calculations presented in this paper consider the 100 mT Feshbach resonance of ^{87}Rb [25]. The underlying concepts can be extended to arbitrary species of Bosonic atoms, while the two-body physics is also applicable to any pair of atoms interacting via s waves, including Fermionic species.

The structure of the paper is as follows: Section II describes the binary physics of the association of ultracold atoms to a diatomic molecule, and Section III analyses the many-body aspects of this process in a Bose-Einstein condensate. Section IV summarises and presents our conclusions, and there is an appendix, which expands upon the explicit description of the binary collision physics specific to this work.

Section II presents a two channel description of the magnetic field tunable resonance enhanced binary scattering and its relationship to the properties of the highest excited vibrational bound state. We develop the concept of a two-body Hamiltonian that accurately describes the relevant physics in terms of a minimal set of five parameters, which can usually be deduced from measurable properties of a Feshbach resonance. We then focus on the near resonance universal properties of the highest excited vibrational bound state, and identify the smooth transition between free and bound atoms in an ideally adiabatic passage across a Feshbach resonance. We then consider the dynamics of the association of just two atoms during a linear ramp of the magnetic field strength across a Feshbach resonance, and reveal the dependence of molecular conversion on the physical parameters. The last subsection is concerned with the determination of dissociation energy spectra, as dissociation of molecules by ramps of the magnetic field strength is frequently a necessary precursor to their detection. We show that both the molecular conversion efficiency and the dissociation spectra are determined by the same physical parameters of a Feshbach resonance, and are subject to a remarkable insensitivity with respect to the details of the binary collision dynamics, provided that the magnetic field strength is varied linearly.

Section III introduces the relevant elements of the microscopic quantum dynamics approach [26], which properly accounts for both the microscopic binary collision physics and the macroscopic coherent nature of an inhomogeneous atomic Bose-Einstein condensate. Using this approach, we study the many-body aspects of the molecular production during a linear adiabatic passage of the magnetic field strength across a Feshbach resonance. From the first order microscopic quantum dynamics approach, by applying the Markov approximation, we derive the commonly used two level mean field model [27, 28, 29, 30, 31, 32, 33, 34, 35]. We discuss the deficits of two level models with respect to the description of the intermediate dynamics during passage of the magnetic field strength across a Feshbach resonance. Our comparative studies show, however, that the many-body approaches predict virtually the same final molecular production at all levels of approximation considered in this paper, provided that the ramp of the magnetic field strength across the Feshbach resonance is linear. We provide the reasons for this universal

ity of the molecular conversion in linear ramps of the magnetic field strength with respect to the details of the underlying microscopic binary collision dynamics and to the coherent nature of the Bose-Einstein condensed gas. We then show that the molecular production efficiency is determined by the same physical parameters that we have previously identified in the associated two-body problem. Our findings strongly indicate that measurements of molecular production efficiencies as well as dissociation spectra obtained from *linear* ramps of the magnetic field strength are largely inconclusive with respect to the details of the underlying binary collision physics.

II. ADIABATIC ASSOCIATION OF TWO ATOMS

We consider a configuration of two atoms exposed to a homogeneous magnetic field whose strength can be varied. The concept underlying the adiabatic association of diatomic molecules in ultracold gases can be understood solely on the basis of binary collision physics. The key feature of this experimental technique is the adiabatic transfer of the zero energy binary scattering state into the highest excited diatomic vibrational bound state. In this section we shall study the binding energies of the diatomic molecules that determine the positions of the Feshbach resonances. We shall then show how the resonance enhanced interatomic collisions can be accurately described in terms of a minimal set of five quantities that can be determined from current experiments. Specifically, we consider the association of two asymptotically free ultracold ^{87}Rb atoms with a total angular momentum quantum number of $F = 1$ and an orientation quantum number of $m_F = +1$, at magnetic field strengths close to the broadest Feshbach resonance at about 100 mT. We shall also study the dissociation of the molecules, which plays an important role in the direct detection of ultracold molecular gases.

A. Feshbach resonances and vibrational bound states in ^{87}Rb

Throughout this paper, we will denote the open scattering channel of two asymptotically free atoms in the ($F = 1, m_F = +1$) electronic ground state as the open channel with an associated reference potential (the background scattering potential) $V_{\text{bg}}(r)$. The dissociation threshold of $V_{\text{bg}}(r)$ is determined by the internal energy of the noninteracting atoms, i.e. twice the energy corresponding to the ($F = 1, m_F = +1$) hyperfine state. When the atoms are exposed to an external homogeneous magnetic field the m_F degeneracy of the atomic hyperfine levels is removed by the Zeeman effect. As a consequence, the potentials associated with the different asymptotic binary scattering channels are shifted with respect to each other. Although in general the interchannel coupling is weak, in the vicinity of certain magnetic field strengths the open channel can be strongly coupled to closed channels. This strong coupling leads to singularities of the s wave scattering length known as Feshbach resonances. Figure 1 (a) shows the theoretically predicted s wave scattering length of two colliding ^{87}Rb atoms in the electronic ground state that are exposed

to a homogeneous magnetic field of strength B . The theoretical calculations use five coupled equations for one open and four closed channels to describe the s -wave collision of two ($F = 1, m_F = +1$) atoms [36]. We use standard methods to solve these equations for either scattering or bound states.

The Feshbach resonances are related to the binding energy of the highest excited vibrational state in a simple way; the singularities of the scattering length in Fig. 1 (a) exactly match those magnetic field strengths that correspond to the zeros of the binding energy with respect to the threshold energy for dissociation into two asymptotically free atoms. Figure 1 (b) gives an overview of the magnetic field dependence of the binding energies of s -wave symmetry molecular states of two ^{87}Rb atoms below the dissociation threshold energy of the open channel.

B. Two channel energy states

The scattering lengths and binding energies in Fig. 1 have been obtained from exact solutions of the multichannel two-body Schrödinger equation as described in Subsection II A. These calculations were performed with a realistic potential matrix that accurately describes the bound and free molecular states over a wide range of energies and magnetic field strengths. Based on these exact considerations, Fig. 1 reveals that the binding energy of the highest excited vibrational state determines the singularities of the scattering length and, in turn, all resonance enhanced low energy scattering properties of two atoms. Collisions in ultracold gases involve only a quite limited range of energies, and the adiabatic association of molecules takes place at magnetic field strengths in the close vicinity of a particular Feshbach resonance. We shall therefore restrict our analysis to an appropriately smaller range of energies and magnetic field strengths around the 100 mT Feshbach resonance.

1. Background scattering

We shall first show how the low energy background scattering can be accurately described in terms of experimentally known physical quantities. At magnetic field strengths asymptotically far from the resonance the interchannel coupling is weak and the highest excited multichannel vibrational bound state can be determined directly from a single channel description with the background scattering potential $V_{\text{bg}}(r)$. Considerations beyond the scope of this paper [37] show that the corresponding binding energy is determined, to an excellent approximation, by the long range asymptotic behaviour of $V_{\text{bg}}(r)$ and the background scattering length a_{bg} , i.e. the scattering length associated with the background scattering potential $V_{\text{bg}}(r)$. Neglecting retardation phenomena, at large interatomic separations $V_{\text{bg}}(r)$ has the universal form $V_{\text{bg}}(r) \sim -C_6/r^6$, where C_6 is the van der Waals dispersion coefficient. The low energy background scattering is determined by the same parameters a_{bg} and C_6 [37]. This universality is due to the fact that at typical ultracold collision ener-

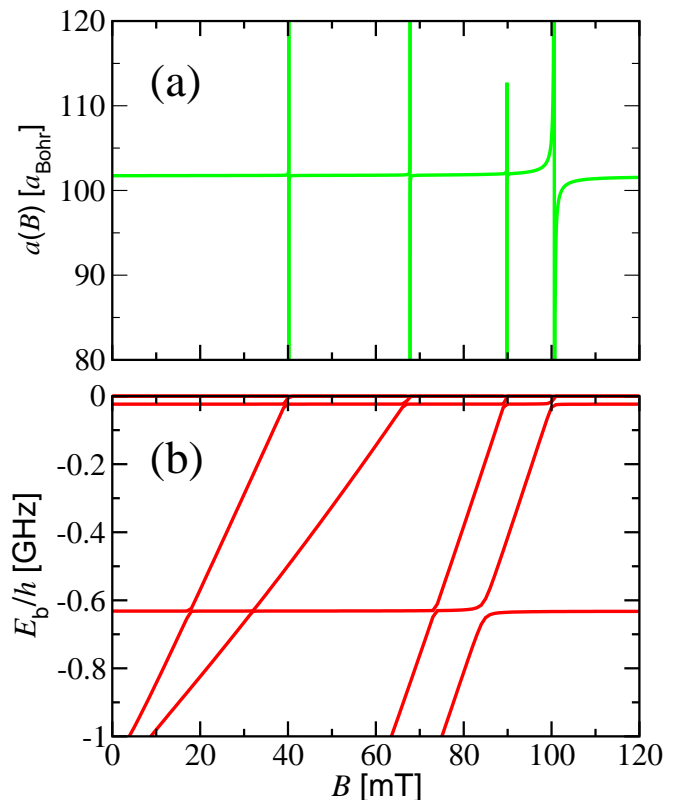


FIG. 1: Magnetic field strength dependence of the s wave scattering length (a) and the energies of the highest excited s -wave vibrational molecular bound states (b) of two ^{87}Rb atoms. At each magnetic field strength B the zero of energy is set at the threshold for dissociation into two asymptotically free atoms in the ($F = 1, m_F = +1$) hyperfine state. The lines in (b) at about -0.02 and -0.63 GHz parallel to the $E = 0$ axis represent the energies of the last s -wave bound states of the open background channel. These states have the same magnetic moment as the separated atoms. The slanted lines in (b) represent closed channel molecular states that have different magnetic moments from the separated atoms. The weak avoided crossings at the intersection of parallel and slanted lines are due to interactions between the background and closed channels, as noted in Ref. [10]. When the closed channel molecular states cross threshold at $E = 0$, the zeros of the binding energy in (b) correspond to the positions of the Feshbach resonances in (a). Our calculated resonance positions are within one per cent of the measured positions [25].

gies the de Broglie wavelengths are much larger than the van der Waals length

$$l_{\text{vdW}} = \frac{1}{2} \left(\frac{mC_6}{\hbar^2} \right)^{1/4}. \quad (1)$$

Here m is the atomic mass. As the van der Waals length is the characteristic length scale set by the long range tail of the background scattering potential, the details of the potential $V_{\text{bg}}(r)$ are not resolved in the collisions. At zero collision energy the background scattering length a_{bg} incorporates all the unresolved details of $V_{\text{bg}}(r)$ into a single length scale. The van der Waals length determines the first correction at finite collision energies, which accounts for the long range asymptotic behaviour of $V_{\text{bg}}(r)$. We note that any model of the back-

ground scattering potential will recover the binding energy of the highest excited vibrational state and all low energy scattering properties of the exact potential $V_{bg}(r)$ to an excellent approximation, if it properly accounts for the parameters C_6 and a_{bg} . We provide an appropriate minimal background scattering potential in the appendix.

2. Two channel Schrödinger equation

We assume in the following that all the bound and free energy states associated with the background scattering potential have been determined, and on this basis derive the resonance enhanced collision properties of two atoms. In the vicinity of a Feshbach resonance, the strong coupling between the open channel and other asymptotic scattering channels originates from the near degeneracy of the magnetic field dependent energy $E_{res}(B)$ of a closed channel vibrational state (a Feshbach resonance level) $\phi_{res}(r)$ with the dissociation threshold energy of the open channel. Consequently, the resonance enhanced collision physics of two ^{87}Rb atoms can be accurately described by the general form of a two-channel Hamiltonian matrix of the relative motion of the atoms:

$$H_{2B} = \begin{pmatrix} -\frac{\hbar^2}{m}\nabla^2 + V_{bg}(r) & W(r) \\ W(r) & -\frac{\hbar^2}{m}\nabla^2 + V_{cl}(B, r) \end{pmatrix}. \quad (2)$$

Here m is the atomic mass, r is the distance between the atoms, $W(r)$ determines the strength of the coupling between the channels, and the closed channel potential $V_{cl}(B, r)$ supports the resonance state:

$$\left[-\frac{\hbar^2}{m}\nabla^2 + V_{cl}(B, r) \right] \phi_{res}(r) = E_{res}(B) \phi_{res}(r). \quad (3)$$

In the following the resonance state $\phi_{res}(r)$ is normalised to unity. In Eq. (2), as elsewhere in this paper, we have chosen the zero of energy as the dissociation threshold of the open channel, i.e. $V_{bg}(r) \xrightarrow{r \rightarrow \infty} 0$. The dissociation threshold of $V_{cl}(B, r)$ is determined accordingly by the energy of two non-interacting atoms in the closed channel that is strongly coupled to the open channel. The relative Zeeman energy shift between the channels can be tuned by varying the magnetic field strength.

The bound and free energy states of the general Hamiltonian matrix in Eq. (2) relate the remaining potentials $W(r)$ and $V_{cl}(B, r)$ to a minimal set of measurable properties of a Feshbach resonance. The two channel states that we shall consider in the following are of the general form $|\text{bg}\rangle\phi_{bg}(\mathbf{r}) + |\text{cl}\rangle\phi_{cl}(\mathbf{r})$, where $|\text{bg}\rangle$ and $|\text{cl}\rangle$ denote the internal states of an atom pair in the open channel and the closed channel strongly coupled to it, respectively. The two components of the energy states are solutions of the stationary coupled Schrödinger equations

$$\left[-\frac{\hbar^2}{m}\nabla^2 + V_{bg}(r) \right] \phi_{bg}(\mathbf{r}) + W(r)\phi_{cl}(\mathbf{r}) = E\phi_{bg}(\mathbf{r}), \quad (4)$$

$$W(r)\phi_{bg}(\mathbf{r}) + \left[-\frac{\hbar^2}{m}\nabla^2 + V_{cl}(B, r) \right] \phi_{cl}(\mathbf{r}) = E\phi_{cl}(\mathbf{r}). \quad (5)$$

3. Continuum states

Bound and continuum energy states are distinguished by their energies and by their asymptotic behaviour at large interatomic distances. In the scattering continuum above the dissociation threshold all energies are in the spectrum of the Hamiltonian in Eq. (2) and can be associated with the momentum \mathbf{p} of the relative motion of two asymptotically noninteracting atoms in the open channel through $E = p^2/m$. Due to the continuous scattering angles between the atoms at a definite collision energy, the scattering energy states are infinitely degenerate. In the following, we will choose their wave functions to behave at large interatomic distances like:

$$\phi_{\mathbf{p}}^{bg}(\mathbf{r}) \underset{r \rightarrow \infty}{\sim} \frac{1}{(2\pi\hbar)^{3/2}} \left[e^{i\mathbf{p}\cdot\mathbf{r}/\hbar} + f(\vartheta, p) \frac{e^{ipr/\hbar}}{r} \right]. \quad (6)$$

This long range asymptotic behaviour corresponds to an incoming plane wave and an outgoing spherical wave in the open channel. Here and throughout this paper we will assume the plane wave momentum states to be normalised as $\exp(i\mathbf{p} \cdot \mathbf{r}/\hbar)/(2\pi\hbar)^{3/2}$. The function $f(\vartheta, p)$ in Eq. (6) is the scattering amplitude, which depends on $p = \sqrt{mE/\hbar^2}$ and on the scattering angle ϑ between the momentum \mathbf{p} of the relative motion of the asymptotically noninteracting incoming atoms and their final relative position \mathbf{r} . The closed channel component $\phi_{\mathbf{p}}^{cl}(\mathbf{r})$ of the wave function vanishes at asymptotically large distances between the colliding atoms. We shall also introduce the energy states $\phi_{\mathbf{p}}^{(+)}(\mathbf{r})$ of the background scattering that satisfy the Schrödinger equation

$$\left[-\frac{\hbar^2}{m}\nabla^2 + V_{bg}(r) \right] \phi_{\mathbf{p}}^{(+)}(\mathbf{r}) = \frac{p^2}{m} \phi_{\mathbf{p}}^{(+)}(\mathbf{r}), \quad (7)$$

with the long range asymptotic behaviour:

$$\phi_{\mathbf{p}}^{(+)}(\mathbf{r}) \underset{r \rightarrow \infty}{\sim} \frac{1}{(2\pi\hbar)^{3/2}} \left[e^{i\mathbf{p}\cdot\mathbf{r}/\hbar} + f_{bg}(\vartheta, p) \frac{e^{ipr/\hbar}}{r} \right]. \quad (8)$$

The coupled Schrödinger equations (4) and (5) can be expressed in terms of the energy dependent Green's functions:

$$G_{bg}(z) = \left[z - \left(-\frac{\hbar^2}{m}\nabla^2 + V_{bg} \right) \right]^{-1}, \quad (9)$$

$$G_{cl}(B, z) = \left[z - \left(-\frac{\hbar^2}{m}\nabla^2 + V_{cl}(B) \right) \right]^{-1}. \quad (10)$$

Here z is a complex parameter with the dimension of an energy. The coupled Schrödinger equations then read:

$$\phi_{\mathbf{p}}^{bg} = \phi_{\mathbf{p}}^{(+)} + G_{bg}(E + i0)W\phi_{\mathbf{p}}^{cl}, \quad (11)$$

$$\phi_{\mathbf{p}}^{cl} = G_{cl}(B, E)W\phi_{\mathbf{p}}^{bg}. \quad (12)$$

The argument “ $z = E + i0$ ” of the Green's function $G_{bg}(z)$ indicates that the physical energy $E = p^2/m$ is approached from the upper half of the complex plane. This choice of the energy argument ensures that the scattering wave function $\phi_{\mathbf{p}}^{bg}(\mathbf{r})$ has the long range asymptotic form of Eq. (6), in accordance with

the asymptotic behaviour of the Green's function at large interatomic distances:

$$G_{bg}(E + i0, \mathbf{r}, \mathbf{r}') \underset{r \rightarrow \infty}{\sim} -(2\pi\hbar)^{3/2} \frac{m}{4\pi\hbar^2} \frac{e^{ipr/\hbar}}{r} [\phi_{\mathbf{p}}^{(-)}(\mathbf{r}')]^*. \quad (13)$$

Here $\phi_{\mathbf{p}}^{(-)}(\mathbf{r}') = [\phi_{-\mathbf{p}}^{(+)}(\mathbf{r}')]^*$ is the incoming continuum energy state associated with the background scattering [38], and $\mathbf{p} = (\sqrt{mE/\hbar^2})\mathbf{r}/r$ can be interpreted as the asymptotic momentum associated with the relative motion of the scattered atoms.

As the resonance state $\phi_{res}(r)$ fulfils the Schrödinger equation (3), according to Eq. (10) the Green's function $G_{cl}(B, z)$ has a singularity at $z = E_{res}(B)$, i.e.

$$\langle \phi_{res} | G_{cl}(B, z) | \phi_{res} \rangle = \frac{1}{z - E_{res}(B)}. \quad (14)$$

At magnetic field strengths in the vicinity of a Feshbach resonance $E_{res}(B)$ is nearly degenerate with the dissociation threshold energy of the open channel. Furthermore, the kinetic energies $E = p^2/m$ in ultracold collisions are small in comparison with the typical spacing between molecular vibrational bound states. As a consequence, the denominator in Eq. (14) becomes sufficiently small for the Green's function $G_{cl}(B, E)$ in Eq. (12) to be excellently approximated by its resonance state component [39]:

$$G_{cl}(B, E) \approx |\phi_{res}\rangle \frac{1}{E - E_{res}(B)} \langle \phi_{res}|. \quad (15)$$

Inserting this pole approximation of the Green's function into Eq. (12) determines the functional form of the closed channel component of the scattering wave function to be

$$|\phi_{\mathbf{p}}^{cl}\rangle = |\phi_{res}\rangle A(B, E). \quad (16)$$

The wave function $\phi_{\mathbf{p}}^{bg}(\mathbf{r})$ is then determined by eliminating $\phi_{\mathbf{p}}^{cl}$ on the right hand side of Eq. (11) in terms of Eq. (16) which gives

$$|\phi_{\mathbf{p}}^{bg}\rangle = |\phi_{\mathbf{p}}^{(+)}\rangle + G_{bg}(E + i0)W|\phi_{res}\rangle A(B, E). \quad (17)$$

The as yet unknown amplitude

$$A(B, E) = \frac{\langle \phi_{res} | W | \phi_{\mathbf{p}}^{bg} \rangle}{E - E_{res}(B)} \quad (18)$$

can be determined straightforwardly by multiplying Eq. (17) by $\langle \phi_{res} | W$ from the left. This yields, after a short calculation:

$$A(B, E) = \frac{\langle \phi_{res} | W | \phi_{\mathbf{p}}^{(+)} \rangle}{E - E_{res}(B) - \langle \phi_{res} | W G_{bg}(E + i0) W | \phi_{res} \rangle}. \quad (19)$$

Once all the energy states associated with the single channel potential $V_{bg}(r)$ and the resonance state $\phi_{res}(r)$ are known, Eqs. (16), (17) and (19) establish the complete solution of the coupled Schrödinger equations (11) and (12) in the pole approximation. Under the assumption that the configuration of

two atoms in the closed channels is restricted to the resonance state ϕ_{res} , the pole approximation becomes exact. This assumption implies the replacement

$$-\frac{\hbar^2}{m} \nabla^2 + V_{cl}(B) \rightarrow |\phi_{res}\rangle E_{res}(B) \langle \phi_{res}| \quad (20)$$

in the two channel Hamiltonian in Eq. (2). Equations (16), (17) and (19) then determine the exact scattering energy states of the resulting restricted two channel Hamiltonian.

The scattering length a is determined by the long range asymptotic form of the scattering wave function $\phi_{\mathbf{p}}^{bg}(\mathbf{r})$ in Eq. (6) through

$$f(\vartheta, p) \underset{p \rightarrow 0}{\sim} -a. \quad (21)$$

Because the incoming plane wave is isotropic at zero energy, this limit is obviously independent of the scattering angle. In an analogous way, the background scattering length a_{bg} is related to the asymptotic form of the scattering wave function $\phi_{\mathbf{p}}^{(+)}(\mathbf{r})$ in Eq. (8), in the limit of zero energy. Inserting the known asymptotic form of the Green's function $G_{bg}(E + i0)$ at large interatomic distances in Eq. (13) and the amplitude in Eq. (19) into Eq. (17), a short calculation determines the scattering length to be:

$$a = a_{bg} - \frac{\frac{m}{4\pi\hbar^2} (2\pi\hbar)^3 |\langle \phi_{res} | W | \phi_0^{(+)} \rangle|^2}{E_{res}(B) + \langle \phi_{res} | W G_{bg}(0) W | \phi_{res} \rangle}. \quad (22)$$

The energy $E_{res}(B)$ of the closed channel state is determined by the Zeeman energy shift between the asymptotic open channel and the closed channel strongly coupled to it. Within the limited range of magnetic field strengths that we shall consider in this paper, the Zeeman effect is approximately linear in the magnetic field strength B . We shall denote by B_{res} the magnetic field strength at which $E_{res}(B)$ crosses the dissociation threshold of the open channel, i.e. $E_{res}(B_{res}) = 0$. An expansion of $E_{res}(B)$ about $B = B_{res}$ yields:

$$E_{res}(B) = \left[\frac{dE_{res}}{dB}(B_{res}) \right] (B - B_{res}). \quad (23)$$

Equations (22) and (23) then determine the magnetic field dependence of the scattering length by the well known formula

$$a(B) = a_{bg} \left[1 - \frac{(\Delta B)}{B - B_0} \right], \quad (24)$$

where

$$(\Delta B) = \frac{m}{4\pi\hbar^2 a_{bg}} \frac{(2\pi\hbar)^3 |\langle \phi_{res} | W | \phi_0^{(+)} \rangle|^2}{\left[\frac{dE_{res}}{dB}(B_{res}) \right]} \quad (25)$$

is termed the resonance width and

$$B_0 = B_{res} - \frac{\langle \phi_{res} | W G_{bg}(0) W | \phi_{res} \rangle}{\left[\frac{dE_{res}}{dB}(B_{res}) \right]} \quad (26)$$

is the measurable resonance position, i.e. the magnetic field strength at which the scattering length has a singularity. We note that according to Eq. (26) the resonance position B_0 is shifted with respect to the magnetic field strength B_{res} at which the energy of the resonance state becomes degenerate with the dissociation threshold energy of the open channel.

4. Bound states

The molecular bound states vanish at asymptotically large interatomic distances, and their energies are below the dissociation threshold of the open channel. Similarly to Eqs. (11) and (12), the coupled Schrödinger equations (4) and (5) can be expressed in terms of the coupled integral equations

$$\phi_b^{\text{bg}} = G_{\text{bg}}(E_b)W\phi_b^{\text{cl}}, \quad (27)$$

$$\phi_b^{\text{cl}} = G_{\text{cl}}(B, E_b)W\phi_b^{\text{bg}}, \quad (28)$$

which incorporate the long range asymptotic behaviour of the components, ϕ_b^{bg} and ϕ_b^{cl} , of the bound state. Here E_b is the binding energy. A short calculation verifies that the pole approximation in Eq. (15) leads to the normalised solutions

$$\begin{pmatrix} \phi_b^{\text{bg}} \\ \phi_b^{\text{cl}} \end{pmatrix} = \frac{1}{\mathcal{N}_b} \begin{pmatrix} G_{\text{bg}}(E_b)W\phi_{\text{res}} \\ \phi_{\text{res}} \end{pmatrix} \quad (29)$$

with the normalisation constant

$$\mathcal{N}_b = \sqrt{1 + \langle \phi_{\text{res}} | W [G_{\text{bg}}(E_b)]^2 W | \phi_{\text{res}} \rangle}, \quad (30)$$

whenever the binding energy E_b fulfils the condition:

$$E_b = E_{\text{res}}(B) + \langle \phi_{\text{res}} | W G_{\text{bg}}(E_b) W | \phi_{\text{res}} \rangle. \quad (31)$$

We note that Eq. (31) recovers Eq. (26) when the binding energy and the magnetic field strength are inserted as $E_b = 0$ and $B = B_0$, respectively, i.e. the binding energy, indeed, vanishes at the position of the resonance.

5. Minimal two channel Hamiltonian

Both the resonance width in Eq. (25) and the shift in Eq. (26) depend only on the product $W(r)\phi_{\text{res}}(r)$. Consequently, for a minimal description of the resonance enhanced scattering we only need to specify $W(r)\phi_{\text{res}}(r)$ in terms of two parameters to recover the magnetic field dependence of the scattering length in Eq. (24) and its relationship with the binding energy of the highest excited vibrational state. A derivation beyond the scope of this paper shows that, once the width of the resonance is known experimentally, a determination of the resonance shift does not require a full solution of the coupled channel two-body Schrödinger equation with a realistic potential matrix. It turns out that Eq. (26) is excellently approximated by [40]

$$B_0 - B_{\text{res}} = (\Delta B) \frac{\frac{a_{\text{bg}}}{a} \left(1 - \frac{a_{\text{bg}}}{a}\right)}{1 + \left(1 - \frac{a_{\text{bg}}}{a}\right)^2}. \quad (32)$$

Here \bar{a} is the mean scattering length of the background scattering potential $V_{\text{bg}}(r)$, which is related to the van der Waals length in Eq. (1) and Euler's Γ function by [41]

$$\bar{a} = \frac{1}{\sqrt{2}} \frac{\Gamma(3/4)}{\Gamma(5/4)} l_{\text{vdW}}. \quad (33)$$

This approximation is consistent with the treatment of the background scattering in terms of just the parameters a_{bg} and l_{vdW} in II B 1.

In addition to the parameters C_6 and a_{bg} of the background scattering potential $V_{\text{bg}}(r)$, a minimal description of the resonance enhanced scattering in a two channel Hamiltonian thus requires us to account for the width (ΔB) in Eq. (25) and the shift $B_0 - B_{\text{res}}$ in Eqs. (26) and (32), in terms of the inter-channel coupling $W(r)\phi_{\text{res}}(r)$, while the slope $\left[\frac{dE_{\text{res}}}{dB}(B_{\text{res}})\right]$ of the resonance in Eq. (23) determines the component of the Hamiltonian in the closed channel that is strongly coupled to the open channel. For the 100 mT Feshbach resonance of ^{87}Rb , four of the five parameters of the two channel Hamiltonian, i.e. $C_6 = 4660$ a.u. [42] (1 a.u. = 0.095734 yJ nm⁶), $a_{\text{bg}} = 100$ a_{Bohr} [43] ($a_{\text{Bohr}} = 0.052918$ nm), $(\Delta B) = 0.02$ mT and $B_0 - B_{\text{res}} = -0.006371$ mT, can be either directly deduced from experiments [44] or from Eq. (32). The only parameter that is not easily accessible is the slope of the resonance. We have obtained $\frac{1}{h} \left[\frac{dE_{\text{res}}}{dB}(B_{\text{res}})\right] = 38$ MHz/mT from the binding energies in Fig. 1. In the appendix we provide the explicit form of the minimal two channel Hamiltonian in the pole approximation that we apply in the following to determine the dynamics of the adiabatic association of molecules. Figure 2 shows the magnetic field dependence of the binding energies as obtained from this minimal Hamiltonian. The low energy scattering properties of two asymptotically free ^{87}Rb atoms in the open channel and the properties of the highest excited vibrational bound state are insensitive with respect to the details of the implementation of the five parameter two channel Hamiltonian.

C. Universal properties of near resonant bound states

We shall now focus on the properties of the highest excited vibrational bound state ϕ_b on the low field side of the Feshbach resonance whose emergence at the resonance position $B_0 = 100.74$ mT causes the singularity of the scattering length (see Fig. 2). The vibrational state ϕ_b is determined by its components in the open channel and in the closed channel strongly coupled to it, as given by Eq. (29), while the binding energy is determined by Eq. (31). We note that the closed channel component $\phi_b^{\text{cl}}(r)$ in Eq. (29) has the functional form of the resonance state $\phi_{\text{res}}(r)$, which we have normalised to unity. Figure 3 shows the population

$$4\pi \int_0^\infty r^2 dr \left| \phi_b^{\text{bg}}(r) \right|^2 = \frac{\mathcal{N}_b^2 - 1}{\mathcal{N}_b^2} \quad (34)$$

of the open channel component of the highest excited vibrational bound state ϕ_b as a function of the magnetic field strength.

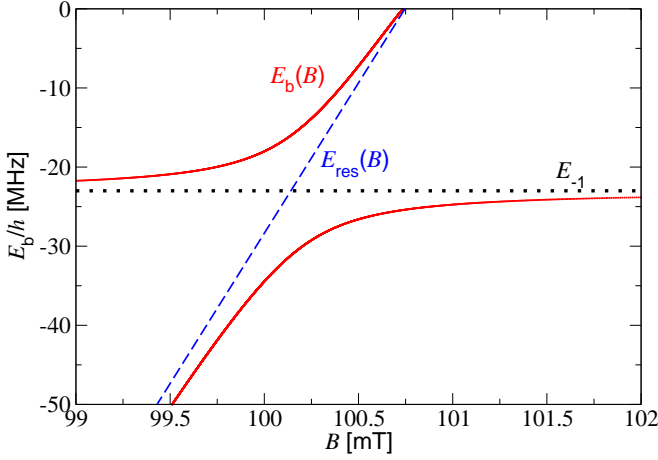


FIG. 2: The magnetic field dependence of the binding energy of the vibrational bound states of the two channel Hamiltonian in the appendix (solid curves). On the low field side of the resonance a new bound state ϕ_b emerges at the resonance position $B_0 = 100.74$ mT [44] whose binding energy we have denoted by $E_b(B)$. At magnetic field strengths asymptotically far from the resonance, the highest excited two channel vibrational bound state becomes identical with the highest excited single channel vibrational bound state $\phi_{-1}(r)$ that is associated with $V_{bg}(r)$ and whose binding energy is denoted by E_{-1} (dotted horizontal line). The dashed line indicates the energy $E_{res}(B)$ of the resonance state.

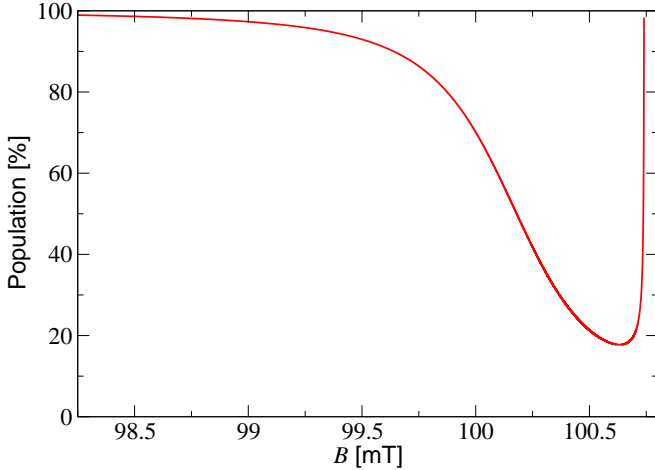


FIG. 3: The population of the open channel component of the highest excited vibrational bound state ϕ_b as a function of the magnetic field strength on the low field side of the Feshbach resonance. The population was determined from the minimal two channel Hamiltonian in the appendix.

At magnetic field strengths asymptotically far from the resonance, Fig. 3 shows that ϕ_b is transferred entirely into the bound state $\phi_{-1}(r)$ of $V_{bg}(r)$, i.e. the highest excited vibrational bound state in the absence of interchannel coupling. Figure 3 also reveals that ϕ_b is dominated by its component in the open channel also in a small region of magnetic field strengths in the close vicinity of the Feshbach resonance.

1. Universal binding energy

We shall study the binding energy E_b that is determined by Eq. (31) in this small region of magnetic field strengths on the low field side of the Feshbach resonance. As the binding energy vanishes at the resonance position, these studies will involve the asymptotic behaviour of Eq. (31) in the limit $E_b \rightarrow 0$. Inserting the resolvent identity [38]

$$G_{bg}(E_b) = G_{bg}(0) - E_b G_{bg}(0) G_{bg}(E_b) \quad (35)$$

as well as Eqs. (23) and (26) into Eq. (31) yields:

$$E_b = \left[\frac{dE_{res}}{dB}(B_{res}) \right] (B - B_0) - E_b \langle \phi_{res} | W G_{bg}(0) G_{bg}(E_b) W | \phi_{res} \rangle. \quad (36)$$

In accordance with Eq. (9), the Green's functions $G_{bg}(0)$ and $G_{bg}(E_b)$ in Eq. (36) can be decomposed into the complete orthogonal set of bound and continuum energy states associated with the background scattering potential $V_{bg}(r)$. These decompositions yield:

$$E_b = \left[\frac{dE_{res}}{dB}(B_{res}) \right] (B - B_0) - E_b \left[\int d\mathbf{p} \frac{|\langle \phi_{res} | W | \phi_{\mathbf{p}}^{(+)} \rangle|^2}{-\frac{p^2}{m} (E_b - \frac{p^2}{m})} + \sum_v \frac{|\langle \phi_{res} | W | \phi_v \rangle|^2}{-E_v (E_b - E_v)} \right]. \quad (37)$$

Here the sum includes the indices $v = -1, -2, -3, \dots$ of all vibrational bound states $\phi_v(r)$ associated with the potential $V_{bg}(r)$. In the limit of vanishing binding energy E_b , the momentum integral on the right hand side of Eq. (37) is singular at $p = 0$. As a consequence, the slowly varying matrix element $\langle \phi_{res} | W | \phi_{\mathbf{p}}^{(+)} \rangle$ can be evaluated at $p = 0$, while the sum over the vibrational bound states can be neglected. Using the general relationship between the matrix element $\langle \phi_{res} | W | \phi_0^{(+)} \rangle$ and the resonance width in Eq. (25), the asymptotic form of the remaining momentum integral is then given by:

$$\int d\mathbf{p} \frac{|\langle \phi_{res} | W | \phi_{\mathbf{p}}^{(+)} \rangle|^2}{-\frac{p^2}{m} (E_b - \frac{p^2}{m})} \underset{E_b \rightarrow 0}{\sim} 4\pi \int_0^\infty p^2 dp \frac{|\langle \phi_{res} | W | \phi_0^{(+)} \rangle|^2}{-\frac{p^2}{m} (E_b - \frac{p^2}{m})} = \left[\frac{dE_{res}}{dB}(B_{res}) \right] (\Delta B) a_{bg} \sqrt{\frac{m}{\hbar^2 |E_b|}}. \quad (38)$$

With this evaluation of the integral, Eq. (37) can be solved for E_b and recovers the universal form

$$E_b(B) = -\frac{\hbar^2}{m[a(B)]^2} \quad (39)$$

of the binding energy.

2. Universal bound states

In accordance with Eq. (29), near resonance the highest excited bound state is strongly dominated by its component in

the asymptotic open channel, which is given by

$$\phi_b(r) = \phi_b^{\text{bg}}(r) = \frac{1}{\sqrt{2\pi a(B)}} \frac{e^{-r/a(B)}}{r} \quad (40)$$

at interatomic distances that are large in comparison with the van der Waals length. This wave function is extended far beyond the outer classical turning point $r_{\text{classical}} = [a(B)(2I_{\text{vdW}})^2]^{1/3}$ of the background scattering potential $V_{\text{bg}}(r)$, with a mean interatomic distance on the order of the scattering length:

$$\langle r \rangle = 4\pi \int_0^\infty r^2 dr |\phi_b(r)|^2 r = a(B)/2. \quad (41)$$

As a consequence, the coupling between the channels in the close vicinity of a Feshbach resonance can be treated, to an excellent approximation, as a perturbation of the background scattering potential $V_{\text{bg}}(r)$. In fact, to describe the universal low energy scattering properties as well as the highest excited vibrational bound state, the whole potential matrix can be replaced by a single channel potential $V(B, r)$ that recovers the correct magnetic field dependence of the scattering length and the length scale associated with the long range van der Waals interaction between the atoms. This involves the replacement of the two-body Hamiltonian matrix in Eq. (2) by the single channel Hamiltonian

$$H_{2\text{B}} = -\frac{\hbar^2}{m} \nabla^2 + V(B, r). \quad (42)$$

Figure 4 shows a comparison between the component ϕ_b^{bg} of the highest excited vibrational bound state as determined from a full multichannel calculation, and from a single channel Hamiltonian with the background scattering potential modified in such a way that it recovers the scattering length of the full multichannel Hamiltonian.

When the magnetic field strength approaches the resonance position from below, the spatial extent of $\phi_b(r)$ becomes infinite and the bound state wave function becomes degenerate with the zero energy scattering state of two asymptotically free atoms in the open channel. Consequently, by sweeping the magnetic field strength adiabatically across the resonance from negative to positive scattering lengths the zero energy scattering state is transferred smoothly into the bound state $\phi_b(r)$. This is the key feature of the adiabatic association of molecules in ultracold atomic gases. We note that applying the sweep of the magnetic field strength in the direction from positive to negative scattering lengths is not suited to associate molecules because there is no energetically accessible vibrational bound state on the high field side of the Feshbach resonance. Both the association mechanism and its asymmetry in the direction of the sweep can be understood purely in terms of two-body considerations.

D. Transition probability

We shall show in the following how the dynamics of the adiabatic association technique can be described in terms of the

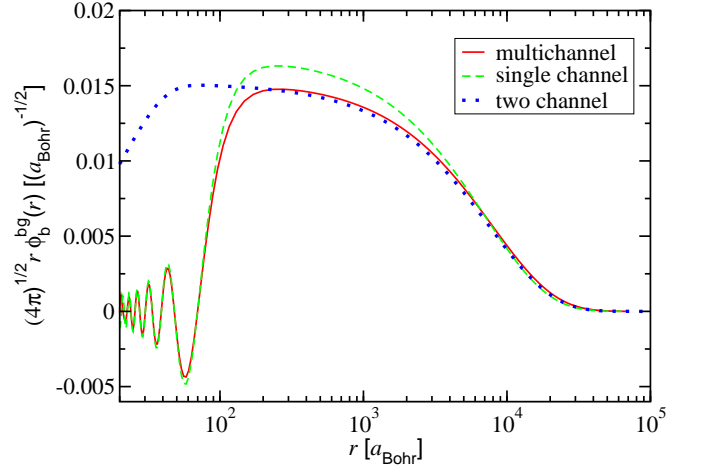


FIG. 4: Radial wave functions associated with the component ϕ_b^{bg} of the highest excited vibrational bound state as determined from a full multichannel calculation (solid curve) and from a single channel Hamiltonian (dashed curve) with the background scattering potential modified in such a way that it recovers the same scattering length $a(B) = 7200 a_{\text{Bohr}}$ as the full multichannel Hamiltonian. The dotted curve shows the result of an analogous calculation with the minimal two channel Hamiltonian in the appendix. The components ϕ_b^{bg} of the two- and multichannel wave functions agree at interatomic distances r that are large in comparison with the van der Waals length of about $80 a_{\text{Bohr}}$. The minimal two channel description does not account for all the bound states of the exact background scattering potential. The nodes of the multichannel wave function are therefore not recovered. The differences between the single channel wave function and the solid and dotted curves result from their different normalisation due to the small but still relevant 10 % admixture of the resonance state in the multichannel wave functions. We note that the radial coordinate is given on a logarithmic scale.

previous considerations. We assume that the magnetic field strength is swept linearly across the resonance position starting asymptotically far from the resonance on the high field side. The two-body Hamiltonian in Eq. (2) becomes explicitly time dependent through its dependence on the magnetic field strength, i.e. $H_{2\text{B}} = H_{2\text{B}}(t)$. The probability for the adiabatic association of a pair of atoms in the initial state $|\Psi_i\rangle$ is determined in terms of the two-body time evolution operator $U_{2\text{B}}(t_f, t_i)$ by:

$$P_{fi} = |\langle \phi_b(B_f) | U_{2\text{B}}(t_f, t_i) | \Psi_i \rangle|^2. \quad (43)$$

Here t_i and t_f are the initial and final times before and after the linear ramp of the magnetic field strength, respectively, while $\phi_b(B_f)$ is the highest excited vibrational bound state of the two-body Hamiltonian $H_{2\text{B}}(t_f)$ at the final magnetic field strength $B(t_f)$. The time evolution operator is determined by the Schrödinger equation:

$$i\hbar \frac{\partial}{\partial t} U_{2\text{B}}(t, t_i) = H_{2\text{B}}(t) U_{2\text{B}}(t, t_i). \quad (44)$$

The transition amplitude in Eq. (43) for the minimal two channel Hamiltonian in the appendix can be obtained with methods similar to those applied to the determination of the single

channel two-body time evolution operator in Ref. [45]. A transition amplitude similar to that in Eq. (43) serves as an input to the microscopic quantum dynamics approach to the association of molecules in a trapped dilute Bose-Einstein condensate that is presented in Subsection III A.

We shall use Eq. (43) to determine the probability for the association of two atoms in the ground state of a large box of volume \mathcal{V} that is later taken to infinity. In the homogeneous limit the appropriate initial state in Eq. (43) is given by the product state

$$|\Psi_i\rangle = |0, \text{bg}\rangle \sqrt{\frac{(2\pi\hbar)^3}{\mathcal{V}}}, \quad (45)$$

where $|0\rangle$ is the isotropic zero momentum plane wave of the relative motion of two atoms in free space and $|\text{bg}\rangle$ denotes their internal state in the asymptotic open channel. The factor $\sqrt{(2\pi\hbar)^3/\mathcal{V}}$ in Eq. (45) provides the appropriate normalisation. In the homogeneous limit the product $P_{fi}\mathcal{V}$ is independent of the volume \mathcal{V} .

Figure 5 shows the product $P_{fi}\mathcal{V}$ as a function of the initial time t_i for a linear sweep of the magnetic field strength across the 100.74 mT Feshbach resonance of ^{87}Rb with a ramp speed of 0.1 mT/ms. The calculations were performed on the basis of Eq. (43) with the two channel approach of the appendix (solid curve) and with a single channel Hamiltonian (dashed curve) that properly accounts for the width of the resonance. Although the detailed time evolution is slightly different in the single and two channel case the transition probabilities are virtually equal once the ramp starts sufficiently far outside the width of the resonance. We shall show in Subsection II E how this independence of the final molecular population from the details of the two-body description can be derived in a systematic way. This derivation will reveal that in the limits $t_i \rightarrow -\infty$ and $t_f \rightarrow \infty$ the product $P_{fi}\mathcal{V}$ depends only on the atomic mass m , the background scattering length a_{bg} , the width of the resonance (ΔB) , and the ramp speed.

E. Landau-Zener approach

An intuitive extension of the two-body dynamics to the adiabatic association of molecules in a dilute Bose-Einstein condensate has been developed by Mies *et al.* [36]. This approach is based on the time dependent two-body Schrödinger equation

$$i\hbar \frac{\partial}{\partial t} \Psi(t) = H_{2\text{B}}(t) \Psi(t) \quad (46)$$

in the spherically symmetric harmonic potential of an optical atom trap [46]. The confining atom trap modifies the potentials in Eq. (2) to $V_{\text{bg}}(r) \rightarrow V_{\text{bg}}(r) + \frac{1}{2} \frac{m}{2} \omega_{\text{ho}}^2 r^2$ and $V_{\text{cl}}(B, r) \rightarrow V_{\text{cl}}(B, r) + \frac{1}{2} \frac{m}{2} \omega_{\text{ho}}^2 r^2$, where ω_{ho} is the angular trap frequency. To extend the binary dynamics to the association of molecules in a dilute Bose-Einstein condensate, Mies *et al.* have formulated Eq. (46) in terms of a basis set expansion with respect to the single channel energy states in the open channel and the closed channel strongly coupled to it. In

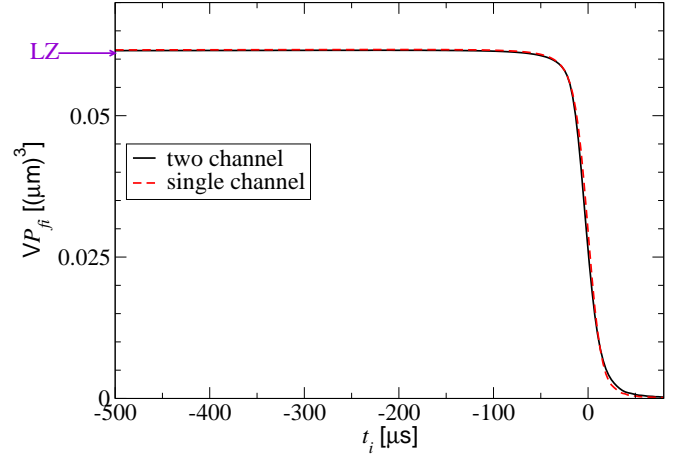


FIG. 5: The product $P_{fi}\mathcal{V}$ as a function of the initial time t_i for two ^{87}Rb atoms in the ground state of a large box with the volume \mathcal{V} . The solid curve shows results based on the two channel approach of the appendix, while the dashed curve corresponds to an analogous calculation with a single channel Hamiltonian that properly accounts for the width of the resonance. The final time in these calculations is $t_f = 80 \mu\text{s}$; $t_i = 0$ corresponds to the initial time at which the linear ramp of the magnetic field strength starts at the position of the Feshbach resonance. In the case of $t_i < 0$ the linear ramp crosses the resonance position from above. The horizontal arrow indicates the asymptotic Landau-Zener prediction for $P_{fi}\mathcal{V}$ as obtained from Eq. (61) in Subsection II E.

this subsection, we shall develop an improved version of this approach.

1. Two-body configuration interaction approach

We label the spherically symmetric energy states associated with the background scattering by the vibrational quantum numbers $v = 0, 1, 2, \dots$. These energy states fulfil the stationary Schrödinger equation

$$\left[-\frac{\hbar^2}{m} \nabla^2 + V_{\text{bg}}(r) \right] \phi_v(r) = E_v \phi_v(r). \quad (47)$$

In contrast to the free space continuum energy states $\phi_{\mathbf{p}}^{(+)}(\mathbf{r})$ in Eq. (8), the vibrational trap states $\phi_v(r)$ are confined in space and we shall assume them to be unit normalised. In the atom trap the dissociation threshold energy in the open channel is given by E_0 . In analogy to Subsection II C we will label the vibrational bound states $\phi_v(r)$ below this threshold by negative quantum numbers $v = -1, -2, -3, \dots$. For realistic atom traps and background scattering potentials, we can presuppose the condition $|E_{-1}| \gg \hbar\omega_{\text{ho}}$ to be fulfilled. As a consequence, the vibrational bound states below the dissociation threshold are hardly modified by the trapping potential. We shall assume furthermore that the configuration of the atoms in the closed channel that is strongly coupled to the open channel, is restricted to the resonance state $\phi_{\text{res}}(r)$. This assumption is analogous to the pole approximation in Eq. (15). The basis

set expansions for the open channel and the closed channel components of $\Psi(t)$ are then given by

$$\Psi_{\text{bg}}(r, t) = \sum_v \phi_v(r) C_v(t) \quad (48)$$

$$\Psi_{\text{cl}}(r, t) = \phi_{\text{res}}(r) C_{\text{res}}(t), \quad (49)$$

respectively. The expansion coefficients $C_v(t)$ and $C_{\text{res}}(t)$ are determined by Eq. (46) in terms of the equivalent infinite set of coupled configuration interaction (CI) equations:

$$i\hbar \dot{C}_v(t) = E_v C_v(t) + \langle \phi_v | W | \phi_{\text{res}} \rangle C_{\text{res}}(t), \quad (50)$$

$$i\hbar \dot{C}_{\text{res}}(t) = E_{\text{res}}(B(t)) C_{\text{res}}(t) + \sum_v \langle \phi_{\text{res}} | W | \phi_v \rangle C_v(t). \quad (51)$$

These equations determine the exact dynamics of the adiabatic association of two atoms in the confining potential of an atom trap.

2. Many-body configuration interaction approach

There are two essential phenomena that should be taken into account to extend the two-body CI approach to the many-body physics of the adiabatic association of molecules in a dilute Bose-Einstein condensate. First, the many-body mean field interactions can cause the size of the atom cloud to occupy a much larger volume than a single atom in the harmonic trapping potential. This size is determined by the nonlinearity parameter $k_{\text{bg}} = Na_{\text{bg}}/l_{\text{ho}}$ of the Gross-Pitaevskii equation [47]. Here N is the number of atoms and $l_{\text{ho}} = \sqrt{\hbar/(m\omega_{\text{ho}})}$ is the oscillator length of the atom trap. We shall assume in the following that the Thomas Fermi condition $k_{\text{bg}} \gg 1$ is fulfilled. This directly implies that the extension of the atom cloud is characterised by the Thomas Fermi radius:

$$l_{\text{TF}} = l_{\text{ho}} (15 k_{\text{bg}})^{1/5}. \quad (52)$$

This radius determines the mean kinetic energy per atom [48]

$$\frac{\langle E_{\text{kin}} \rangle}{N} = \hbar\omega_{\text{ho}} \frac{5}{2} \left(\frac{l_{\text{ho}}}{l_{\text{TF}}} \right)^2 \ln \left(\frac{l_{\text{TF}}}{1.2683 l_{\text{ho}}} \right). \quad (53)$$

The physical intuition underlying the Thomas Fermi limit relies upon the observation that the mean field potential cancels the trap potential at distances smaller than the Thomas Fermi radius. Under these assumptions the single atoms experience an effective flat potential rather than the harmonic potential of the atom trap. Motivated by this physical intuition, Mies *et al.* replaced the vibrational trap states in the matrix elements in Eqs. (50) and (51) by those that correspond to a spherical box with a zero point energy of $\langle E_{\text{kin}} \rangle / N$. The radius of this box is then determined by:

$$l_{\text{box}} = l_{\text{TF}} \left(\frac{2}{5} \right)^{1/2} \frac{\pi}{\sqrt{\ln \left(\frac{l_{\text{TF}}}{1.2683 l_{\text{ho}}} \right)}}. \quad (54)$$

The second many-body phenomenon taken into account by Mies *et al.* is the macroscopic occupation of the lowest energy mode corresponding to the Bose-Einstein condensate. Neglecting the curve crossing between $E_{\text{res}}(B)$ and the energy E_{-1} of the highest excited bound state of the background scattering potential in Fig. 2, in a downward ramp of the magnetic field strength across the Feshbach resonance the prevailing asymptotic transition involves only the condensate mode and the resonance state. As each atom has $N - 1$ atoms to interact with, the element of the potential matrix that is associated with this prevailing transition is enhanced by a factor of $\sqrt{N - 1}$.

Combining these results leads to a two level Rabi flopping model for the adiabatic association of molecules in a Bose-Einstein condensate:

$$i\hbar \dot{C}_0(t) = E_0 C_0(t) + \frac{1}{2} \hbar \Omega^* C_{\text{res}}(t), \quad (55)$$

$$i\hbar \dot{C}_{\text{res}}(t) = E_{\text{res}}(B(t)) C_{\text{res}}(t) + \frac{1}{2} \hbar \Omega C_0(t). \quad (56)$$

Here the Rabi frequency is given by

$$\Omega = 2 \sqrt{N - 1} \frac{1}{\hbar} \sqrt{\frac{(2\pi\hbar)^3}{3 l_{\text{box}}^3}} \langle \phi_{\text{res}} | W | \phi_0^{(+)} \rangle. \quad (57)$$

We note that we have quoted the Rabi frequency in terms of the free space zero energy background scattering state $\phi_0^{(+)}(\mathbf{r})$ as introduced in Eq. (8). The factor $\sqrt{(2\pi\hbar)^3 / (\frac{4\pi}{3} l_{\text{box}}^3)}$ provides the proper normalisation that accounts for the finite volume $\mathcal{V} = \frac{4\pi}{3} l_{\text{box}}^3$ of the box. In accordance with Eq. (25), the matrix element $\langle \phi_{\text{res}} | W | \phi_0^{(+)} \rangle$ in Eq. (57) can be expressed in terms of the resonance width (ΔB) , the slope $\left[\frac{dE_{\text{res}}}{dB}(B_{\text{res}}) \right]$ of the resonance and the background scattering length a_{bg} .

When the magnetic field strength is swept linearly across the Feshbach resonance the energy of the resonance state changes linearly in time:

$$E_{\text{res}}(B(t)) = E_0 + \left[\frac{dE_{\text{res}}}{dB}(B_{\text{res}}) \right] \left[\frac{dB}{dt}(t_{\text{res}}) \right] (t - t_{\text{res}}). \quad (58)$$

Here t_{res} is the time at which the energy of the resonance state crosses the dissociation threshold energy of the open channel, i.e. $B(t_{\text{res}}) = B_{\text{res}}$ and $E_{\text{res}}(B_{\text{res}}) = E_0$. Under the assumption of a linear Feshbach resonance crossing with the initial populations $|C_0(t_i)|^2 = 1$ and $|C_{\text{res}}(t_i)|^2 = 0$, the final populations $|C_0(t_f)|^2$ and $|C_{\text{res}}(t_f)|^2$ can be determined by the Landau-Zener formulae:

$$|C_0(t_f)|^2 = e^{-2\pi\delta_{\text{LZ}}}, \quad (59)$$

$$|C_{\text{res}}(t_f)|^2 = 1 - e^{-2\pi\delta_{\text{LZ}}}, \quad (60)$$

in the limits $t_i \rightarrow -\infty$ and $t_f \rightarrow \infty$. Derivation of the asymptotic Landau-Zener populations requires much tedious calculation. Given the known general form of the exponent δ_{LZ} , however, a short calculation using Eq. (25) reveals its simple

dependence on the background scattering length a_{bg} , the resonance width (ΔB) and the ramp speed $|\frac{dB}{dt}(t_{res})|$:

$$\delta_{LZ} = \frac{\hbar|\Omega|^2}{4|\frac{dE_{res}}{dB}(B_{res})||\frac{dB}{dt}(t_{res})|} = \frac{(N-1)4\pi\hbar|a_{bg}||\Delta B|}{\mathcal{V}m|\frac{dB}{dt}(t_{res})|}. \quad (61)$$

Although Eq. (61) can be derived on the basis of the simple two level Rabi flopping model in Eqs. (55) and (56), the two-body ($N = 2$) Landau-Zener prediction is accurate even in applications to transition probabilities that include a continuum of energy levels above the dissociation threshold (see Fig. 5). In fact, the Landau-Zener coefficient for the asymptotic population of the resonance state $\phi_{res}(r)$ can be derived rigorously for an arbitrary number of linear curve crossings associated with a quasi continuum of two-body energy states [49]. We note, however, that despite the universality of the asymptotic populations, a two level model is not suited to provide an adequate description of the intermediate states and their intermediate populations. From this viewpoint, the agreement between the asymptotic two- and multilevel descriptions is coincidental.

When applied to a gas of many atoms the linear two level Rabi flopping model in Eqs. (55) and (56) yields analytic predictions on the efficiency of molecular production. The treatment of the Bose enhancement in the linear model, however, does not account for the depletion of the condensate mode in the course of the adiabatic association. This depletion can be accounted for in a straightforward way by replacing the initial number of condensate atoms N by the actual number $N|C_0(t)|^2$ in the enhancement factor. This inclusion of the depletion modifies the linear Rabi flopping model in Eqs. (55) and (56) to the nonlinear dynamic equations:

$$i\hbar\dot{C}_0(t) = E_0C_0(t) + \frac{1}{2}\hbar\Omega^*|C_0(t)|C_{res}(t), \quad (62)$$

$$i\hbar\dot{C}_{res}(t) = E_{res}(B(t))C_{res}(t) + \frac{1}{2}\hbar\Omega|C_0(t)|C_0(t). \quad (63)$$

At final times $t_f \rightarrow \infty$ we shall interpret $N|C_0(t_f)|^2$ as the number of atoms in the remnant Bose-Einstein condensate and $N|C_{res}(t_f)|^2$ as the number of atoms converted into molecules. The number of diatomic molecules produced in the adiabatic association is then given by $N|C_{res}(t_f)|^2/2$. We show in Subsection III C that Eqs. (62) and (63) significantly improve the predictions of the asymptotic Landau-Zener formulae in Eqs. (59) and (60), in particular when the molecular production begins to saturate.

F. Dissociation of molecules

We note that the chemical bond of the diatomic molecules shifts the atomic spectral lines. This line shift can prevent the bound atoms from scattering light of probe lasers even in the case of the very weakly bound Feshbach molecules that are produced with the adiabatic association technique. As a consequence, many present day experimental molecular detection schemes rely upon the spatial separation of bound and

free atoms in the cloud and the subsequent dissociation of the molecules (cf., e.g., Ref. [10]). The highest excited vibrational molecular bound state can be dissociated by crossing the Feshbach resonance from positive to negative scattering lengths which corresponds to an upward ramp in the case of the 100 mT Feshbach resonance of ^{87}Rb . The crossing of the Feshbach resonance transfers the bound molecules into correlated pairs of atoms which can have a comparatively high relative velocity, depending on the ramp speed. In the following we shall characterise the dissociation energy spectra for the 100 mT Feshbach resonance of ^{87}Rb , under the assumption that many-body phenomena can be neglected. We expect this assumption to be accurate because the final continuum states of the molecular fragments have a low occupancy. Consequently, phenomena related to Bose enhancement should be negligible.

1. General determination of dissociation energy spectra

We shall consider linear upward ramps from the initial magnetic field strength B_i at time t_i across the Feshbach resonance to the final field strength B_f at time t_f . Starting from the highest excited multichannel vibrational molecular bound state $\phi_b(B_i)$ at the magnetic field strength B_i , the state of a pair of atoms at any time t is determined in terms of the time evolution operator in Eq. (44) by:

$$\Psi(t) = U_{2B}(t, t_i)\phi_b(B_i). \quad (64)$$

The dissociation energy spectrum is usually measured in a time of flight experiment that allows the fragments to evolve freely after the final time t_f of the ramp. At any time t after t_f the two-body Hamiltonian is stationary, and the time evolution operator can be factorised into its contribution of the linear ramp of the magnetic field strength and a part that describes the subsequent relative motion of a pair of atoms:

$$U_{2B}(t, t_i) = U_{2B}(t - t_f)U_{2B}(t_f, t_i). \quad (65)$$

Here $U_{2B}(t - t_f)$ is determined in terms of the stationary two-body Hamiltonian $H_{2B}(B_f)$ at the final magnetic field strength B_f by:

$$U_{2B}(t - t_f) = e^{-iH_{2B}(B_f)(t-t_f)/\hbar}. \quad (66)$$

We shall insert Eq. (65) into Eq. (64) and represent the time evolution operator of the relative motion of a pair of atoms after the time t_f in terms of the complete set of multichannel energy states at the final magnetic field strength B_f . The state $\Psi(t)$ can then be decomposed as

$$\Psi(t) = \Psi_{free}(t) + \Psi_{bound}(t), \quad (67)$$

where $\Psi_{free}(t)$ describes the dissociation into two asymptotically free fragments, while $\Psi_{bound}(t)$ describes those events in which the bound state $\phi_b(B_i)$ is transferred into more tightly bound multichannel molecular vibrational states at the final magnetic field strength B_f . It is the continuum part $\Psi_{free}(t)$ of the wave function $\Psi(t)$ that determines the measurable dissociation energy spectrum. In terms of the continuum

multichannel energy states $\phi_{\mathbf{p}}(B_f)$ at the final magnetic field strength B_f this is given by

$$\Psi_{\text{free}}(t) = \int d\mathbf{p} \phi_{\mathbf{p}}(B_f) e^{-iE(t-t_f)/\hbar} \langle \phi_{\mathbf{p}}(B_f) | U_{2B}(t_f, t_i) | \phi_{\mathbf{b}}(B_i) \rangle. \quad (68)$$

Here $E = p^2/m$ is the energy of the relative motion of the fragments that corresponds to their relative momentum \mathbf{p} . From Eq. (68) we deduce the probability of detecting a pair of atoms with a relative energy between E and $E + dE$ to be:

$$n(E)dE = p^2 dp \int d\Omega_{\mathbf{p}} |\langle \phi_{\mathbf{p}}(B_f) | U_{2B}(t_f, t_i) | \phi_{\mathbf{b}}(B_i) \rangle|^2. \quad (69)$$

Here $d\Omega_{\mathbf{p}}$ denotes the angular component of $d\mathbf{p}$.

2. Exact dissociation energy spectra

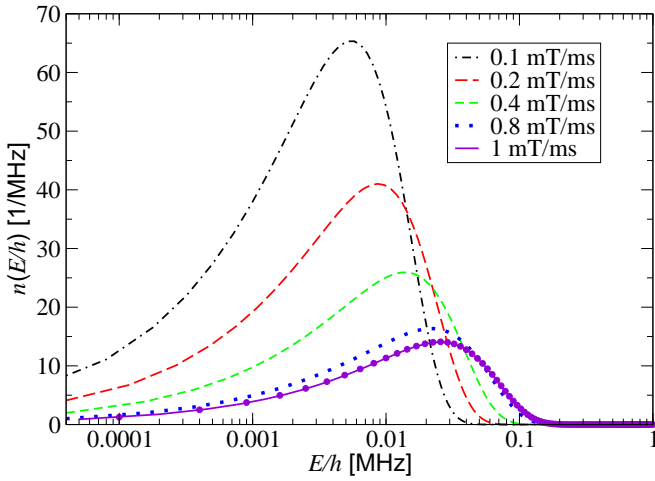


FIG. 6: Dissociation spectra of the highest excited vibrational bound state of $^{87}\text{Rb}_2$ as a function of the relative energy of the fragments. The speeds of the upward ramps across the 100 mT Feshbach resonance were varied between 0.1 mT/ms (dashed dotted curve) and 1 mT/ms (solid curve). The spectra are rather insensitive to the range of magnetic field strengths covered by the ramp; the solid curve indicates a 1 mT/ms ramp with $B_i = 100.7$ mT and $B_f = 100.78$ mT, while the data indicated by the dots on top of the solid curve correspond to a calculation for a 1 mT/ms ramp with initial and final magnetic field strengths that are half way closer to the resonance position of $B_0 = 100.74$ mT. We note that the energies are given on a logarithmic scale.

Figure 6 shows the spectral density $n(E)$ for different ramp speeds as obtained from an exact solution of the Schrödinger equation (44) with the low energy two channel Hamiltonian in the appendix. Although the low energy two-body Hamiltonian supports a comparatively tightly bound state at the high field side of the Feshbach resonance (see Fig. 2), the calculations do not indicate any transfer into this state for the realistic ramp speeds under consideration. Within this range of ramp speeds between 0.1 and 1 mT/ms, the spectra cover a broad range

of energies of the relative motion of a pair of atoms that is much larger than the typical energy spread of a Bose-Einstein condensate. Consequently, the molecular fragments will be detected as a burst of correlated pairs of atoms moving radially outward from the original position of the molecular cloud.

3. Dependence on the physical parameters of a Feshbach resonance

In the following, we shall study in more detail the dependencies of the dissociation spectra in Fig. 6 on the five physical parameters of a Feshbach resonance (cf. Subsection II B), which completely characterise the resonance enhanced low energy collision physics. To this end, we shall neglect the vibrational bound states of the background scattering potential and reformulate Eq. (69) in terms of the energy states in the absence of interchannel coupling, in the formal asymptotic limits $t_i \rightarrow -\infty$ and $t_f \rightarrow \infty$. The idealising assumption that the background scattering potential does not support any vibrational bound states implies that the two channel Hamiltonian in Eq. (2) supports just the initial vibrational bound state $\phi_{\mathbf{b}}(B_i)$ of Eq. (69). In the formal limit $t_i \rightarrow -\infty$, i.e. when the linear ramp of the magnetic field strength starts asymptotically far from the resonance position, $\phi_{\mathbf{b}}(B_i)$ is then identical to the closed channel resonance state ϕ_{res} . Furthermore, in accordance with Eqs. (16), (17) and (19), the final continuum state $\phi_{\mathbf{p}}(B_f)$ of Eq. (69) is transferred into the energy state $\phi_{\mathbf{p}}^{(+)}$ of the background scattering [cf. Eq. (8)], in the formal limit $t_f \rightarrow \infty$. Under these assumptions, Eq. (69) can be reformulated to be

$$n(E)dE = p^2 dp \int d\Omega_{\mathbf{p}} |\langle \phi_{\mathbf{p}}^{(+)} | \text{bg} | U_{2B}(t_f, t_i) | \phi_{\text{res}}, \text{cl} \rangle|^2. \quad (70)$$

Here $|\text{bg}\rangle$ and $|\text{cl}\rangle$ denote the internal states of an atom pair in the asymptotic open channel and the closed channel strongly coupled to it, respectively. The asymptotic dissociation spectrum in Eq. (70) can then be determined from the results of Ref. [49] in analogy to the derivation of the Landau-Zener formulae of Subsection II E. This yields the analytic result for the spectral density [50]:

$$n(E) = -\frac{\partial}{\partial E} \exp \left(-\frac{4}{3} \sqrt{\frac{mE}{\hbar^2}} |a_{\text{bg}}| \frac{E|\Delta B|}{\hbar \left| \frac{dB}{dt}(t_{\text{res}}) \right|} \right). \quad (71)$$

We note that the asymptotic energy density of the dissociation spectrum in Eq. (71) depends, like the Landau-Zener coefficient in Eq. (61), only on those physical parameters that determine the universal low energy scattering properties in the close vicinity of a Feshbach resonance (cf. Subsection II C), while the slope $\left[\frac{dE_{\text{res}}}{dB}(B_{\text{res}}) \right]$ of the resonance and the van der Waals dispersion coefficient C_6 do not contribute to Eq. (71). This corroborates the observation in Fig. 5 that the relevant physics occurs in a small region of magnetic field strengths in which the modulus of the scattering length by far exceeds all the other length scales set by the binary interactions. In our applications to the 100 mT Feshbach resonance of ^{87}Rb ,

the results obtained from Eq. (71) are virtually indistinguishable from those of the exact calculations in Fig. 6. We note, however, that Eq. (71) may not be applicable when the ramp of the magnetic field strength starts in the close vicinity of a Feshbach resonance. This situation may occur, for instance, in experimental applications involving the broad $[(\Delta B) = 1.1 \text{ mT}]$ resonance of ^{85}Rb at 15.5 mT [51].

4. Mean kinetic energy

In the following, we shall study the mean kinetic energies

$$\langle E_{\text{kin}} \rangle = \frac{1}{2} \int_0^\infty dE E n(E) \quad (72)$$

of the molecular fragments after the dissociation. These energies characterise the speed of expansion of the gas of molecular fragments before the detection in related experiments [10]. We note that the kinetic energy of a single atom is $E_{\text{kin}} = p^2/(2m)$, which is half the energy of the relative motion of a pair. Equations (71) and (72) allow us to represent $\langle E_{\text{kin}} \rangle$ in terms of physical parameters of a Feshbach resonance, of the ramp speed and of Euler's Γ function:

$$\langle E_{\text{kin}} \rangle = \frac{1}{3} \left[\frac{3}{4} \sqrt{\frac{\hbar^2}{m(a_{\text{bg}})^2} \frac{\hbar \left| \frac{dB}{dt}(t_{\text{res}}) \right|}{|\Delta B|}} \right]^{2/3} \Gamma(2/3). \quad (73)$$

We expect this prediction to be accurate provided that the initial and final magnetic field strengths of the linear ramp are asymptotically far from the resonance position.

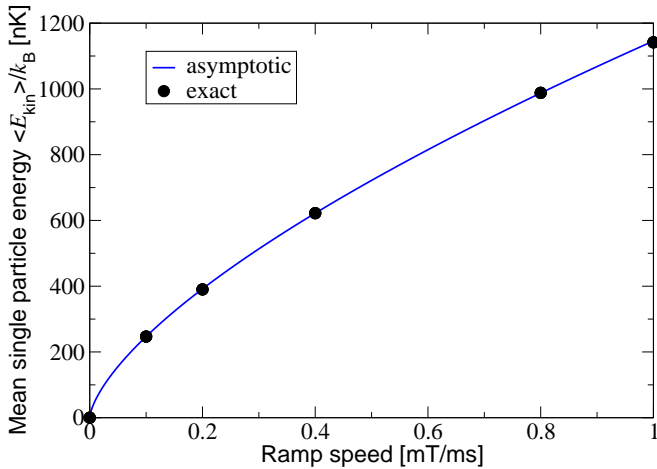


FIG. 7: Mean single particle kinetic energies of the molecular fragments associated with the exact dissociation spectra in Fig. 6 (circles) in dependence on the ramp speed. The solid curve has been obtained from the asymptotic prediction in Eq. (73). The single particle kinetic energy is half the energy of the relative motion of the fragments in Fig. 6.

Figure 7 shows the strong dependence of the mean single particle kinetic energies on the ramp speed. The circles indicate the mean energies of the exact dissociation energy spectra in Fig. 6, while the solid curve has been obtained from

Eq. (73). Both approaches lead to virtually the same predictions for the realistic ramp speeds and physical parameters of the 100 mT Feshbach resonance of ^{87}Rb . Figure 7 also reveals that ramp speeds of less than about 0.03 mT/ms would be required to suppress the mean single particle energies of the fragments to a range below $\langle E_{\text{kin}} \rangle / k_B = 100 \text{ nK}$ ($k_B = 1.3806503 \times 10^{-23} \text{ J/K}$), which would be close to the typical energy spread in a Bose-Einstein condensate [47].

III. ADIABATIC ASSOCIATION OF MOLECULES IN A TRAPPED BOSE-EINSTEIN CONDENSATE

The results in Subsection IID allow us to rigorously treat the two-body physics of the adiabatic association. In this section we shall study the many-body physics of the molecular production in a trapped dilute Bose-Einstein condensate. Inhomogeneous Bose-Einstein condensates are subject to a rich spectrum of collective energy modes that depend sensitively on the number of condensate atoms and their binary interactions, as well as on the confining atom trap. The crossing of a singularity of the scattering length leads to a dramatic change of the intermediate collision physics that transfers a substantial fraction of the initially coherent atomic cloud into strongly correlated pairs of atoms in the highest excited vibrational bound state. This violent dynamics can be expected to couple all energy modes. A proper description of the complex interplay between the macroscopic collective behaviour and the microscopic binary collision physics requires a full many-body treatment. We shall provide an appropriate many-body description of the adiabatic association of molecules in a trapped dilute Bose-Einstein condensate and compare it to previous theoretical predictions at different levels of approximation. This will highlight in what parameter regimes approximate descriptions are valid and to which physical observables they are applicable, as well as when we expect them to break down.

A. Microscopic quantum dynamics approach

The general many-body approach to the dynamics of atomic gases that we shall apply has been derived in Refs. [26, 45]. This approach has been applied previously to several different physical situations that involve the production of correlated pairs of atoms in four wave mixing experiments with Bose-Einstein condensates [26], the determination of the mean field energy associated with three-body collisions [52], and the dynamics of atom molecule coherence [45, 53] as well as Feshbach resonance crossing experiments with degenerate Bose gases of ^{85}Rb and ^{23}Na atoms [54]. The underlying method of cumulants [26, 55] is based on the exact time dependent many-body Schrödinger equation. As the general technique has been derived before, we shall outline only those details specific to the adiabatic association of molecules in a Bose-Einstein condensate.

1. Multichannel approach

We shall formulate the approach in terms of the full multi-channel many-body Hamiltonian, which couples all the internal hyperfine states of the single atoms. We label the quantum numbers associated with the single atom energy states by

$$H = \sum_{\mu} \int d\mathbf{x} \psi_{\mu}^{\dagger}(\mathbf{x}) H_{\mu}^{1B}(B) \psi_{\mu}(\mathbf{x}) + \frac{1}{2} \sum_{\mu\nu\kappa\lambda} \int d\mathbf{x} d\mathbf{y} \psi_{\mu}^{\dagger}(\mathbf{x}) \psi_{\nu}^{\dagger}(\mathbf{y}) V_{\{\mu\nu\},\{\kappa\lambda\}}(\mathbf{x} - \mathbf{y}) \psi_{\kappa}(\mathbf{x}) \psi_{\lambda}(\mathbf{y}). \quad (74)$$

Here the single particle annihilation and creation field operators satisfy the Bose commutation rules:

$$[\psi_{\mu}(\mathbf{x}), \psi_{\nu}^{\dagger}(\mathbf{y})] = \delta_{\mu\nu} \delta(\mathbf{x} - \mathbf{y}), \quad (75)$$

$$[\psi_{\mu}(\mathbf{x}), \psi_{\nu}(\mathbf{y})] = 0. \quad (76)$$

Furthermore, $H_{\mu}^{1B}(B)$ is the one body Hamiltonian associated with the internal atomic state μ that contains the kinetic energy of the atom, the external potential of the optical atom trap, and the internal hyperfine energy $E_{\mu}^{\text{hf}}(B)$:

$$H_{\mu}^{1B}(B) = -\frac{\hbar^2}{2m} \nabla^2 + V_{\text{trap}} + E_{\mu}^{\text{hf}}(B). \quad (77)$$

The hyperfine energy depends on the magnetic field strength through the Zeeman effect. The microscopic binary potential $V_{\{\mu\nu\},\{\kappa\lambda\}}(\mathbf{r})$ in Eq. (74) is associated with the asymptotic incoming and outgoing binary scattering channels that can be labelled by the pairs of internal atomic quantum numbers $\{\kappa\lambda\}$ and $\{\mu\nu\}$, respectively. We note that in this general formulation of the many-body Hamiltonian all potentials associated with the asymptotic binary scattering channels are chosen to vanish at infinite interatomic distances.

All physical properties of a gas of atoms are determined by correlation functions, i.e. quantum expectation values (denoted by $\langle \cdot \rangle_t$) of normal ordered products of field operators for the quantum state at time t . The correlation functions

Greek indices. In our applications to the low energy scattering in the vicinity of the 100 mT Feshbach resonance of ^{87}Rb , these indices are sufficiently characterised by the total angular momentum quantum number F and its orientation quantum number m_F . In its second quantised form, the full many-body Hamiltonian then reads:

of main interest in the adiabatic association of molecules involve the atomic mean field $\langle \psi_{\mu}(\mathbf{x}) \rangle_t$, the anomalous average $\langle \psi_{\nu}(\mathbf{y}) \psi_{\mu}(\mathbf{x}) \rangle_t$, and the one-body density matrix $\langle \psi_{\nu}^{\dagger}(\mathbf{y}) \psi_{\mu}(\mathbf{x}) \rangle_t$. The dynamics of the correlation functions is determined by the many-body Schrödinger equation through an infinite hierarchy of coupled dynamic equations. The cumulant approach consists in transforming the coupled set of dynamic equations for the correlation functions into an equivalent but more practical infinite set of dynamic equations for noncommutative cumulants [26, 45]. The transformed equations of motion for the cumulants can be truncated, at any desired degree of accuracy, in accordance with Wick's theorem of statistical mechanics [56]. The noncommutative cumulants that we shall consider in the following are the atomic mean field

$$\Psi_{\mu}(\mathbf{x}, t) = \langle \psi_{\mu}(\mathbf{x}) \rangle_t, \quad (78)$$

the pair function

$$\Phi_{\mu\nu}(\mathbf{x}, \mathbf{y}, t) = \langle \psi_{\nu}(\mathbf{y}) \psi_{\mu}(\mathbf{x}) \rangle_t - \Psi_{\mu}(\mathbf{x}, t) \Psi_{\nu}(\mathbf{y}, t), \quad (79)$$

and the density matrix of the noncondensed fraction

$$\Gamma_{\mu\nu}(\mathbf{x}, \mathbf{y}, t) = \langle \psi_{\nu}^{\dagger}(\mathbf{y}) \psi_{\mu}(\mathbf{x}) \rangle_t - \Psi_{\mu}(\mathbf{x}, t) \Psi_{\nu}^*(\mathbf{y}, t). \quad (80)$$

In the first order cumulant approach [26, 45] that we shall apply in this paper the atomic mean field and the pair function are determined by the coupled dynamic equations:

$$i\hbar \frac{\partial}{\partial t} \Psi_{\mu}(\mathbf{x}, t) = H_{\mu}^{1B}(B) \Psi_{\mu}(\mathbf{x}, t) + \sum_{\nu\kappa\lambda} \int d\mathbf{y} \Psi_{\nu}^*(\mathbf{y}, t) V_{\{\mu\nu\},\{\kappa\lambda\}}(\mathbf{x} - \mathbf{y}) [\Phi_{\kappa\lambda}(\mathbf{x}, \mathbf{y}, t) + \Psi_{\kappa}(\mathbf{x}, t) \Psi_{\lambda}(\mathbf{y}, t)] \quad (81)$$

$$i\hbar \frac{\partial}{\partial t} \Phi_{\mu\nu}(\mathbf{x}, \mathbf{y}, t) = \sum_{\kappa\lambda} [H_{\{\mu\nu\},\{\kappa\lambda\}}^{2B}(B) \Phi_{\kappa\lambda}(\mathbf{x}, \mathbf{y}, t) + V_{\{\mu\nu\},\{\kappa\lambda\}}(\mathbf{x} - \mathbf{y}) \Psi_{\kappa}(\mathbf{x}, t) \Psi_{\lambda}(\mathbf{y}, t)]. \quad (82)$$

Here $H_{2B}(B)$ is the Hamiltonian matrix of two atoms whose matrix elements

$$H_{\{\mu\nu\},\{\kappa\lambda\}}^{2B}(B) = [H_{\mu}^{1B}(B) + H_{\nu}^{1B}(B)] \delta_{\kappa\mu} \delta_{\lambda\nu} + V_{\{\mu\nu\},\{\kappa\lambda\}} \quad (83)$$

involve all incoming and outgoing asymptotic binary scattering channels associated with the pairs of atomic indices $\{\kappa\lambda\}$ and $\{\mu\nu\}$, respectively. Given the solution of Eqs. (81) and (82), the density matrix of the noncondensed fraction is deter-

mined in terms of the pair function by [45]

$$\Gamma_{\mu\nu}(\mathbf{x}, \mathbf{x}', t) = \sum_{\kappa} \int d\mathbf{y} \Phi_{\mu\kappa}(\mathbf{x}, \mathbf{y}, t) \Phi_{\nu\kappa}^*(\mathbf{x}', \mathbf{y}, t). \quad (84)$$

The general first order dynamic equations (81), (82) and (84) not only strictly conserve the total number of atoms

$$N = \sum_{\mu} \int d\mathbf{x} [\Gamma_{\mu\mu}(\mathbf{x}, \mathbf{x}, t) + |\Psi_{\mu}(\mathbf{x}, t)|^2] \quad (85)$$

at all times, but the explicit form of Eq. (84) also ensures the crucial property of positivity of the one-body density matrix.

Equation (84) reveals that the density of the noncondensed fraction stems directly from the pair function. Consequently, the build up of pair correlations is the main source of atom loss from a Bose-Einstein condensate. The energy delivered by a time dependent homogeneous magnetic field can transfer a pair of condensate atoms either into the highest excited

vibrational molecular bound state or into the quasi continuum of two-body energy states above the dissociation threshold. Not only the molecular association, but also the production of correlated pairs of atoms in the scattering continuum has been observed recently [7] as a burst of atoms ejected from the remnant condensate. As a time dependent homogeneous magnetic field delivers energy but no momentum to the gas, the centres of mass of all correlated bound and free pairs of atoms have the same momentum distribution as the initial Bose-Einstein condensate. In this sense, the molecules produced in the adiabatic association may be considered as a degenerate quantum gas. The number N_b of diatomic molecules in the state ϕ_b is determined by counting the overlap of each pair of atoms with the multichannel molecular bound state [57]. This relates the number of molecules to the two-body correlation function

$$G_{\mu\nu\kappa\lambda}^{(2)}(\mathbf{x}, \mathbf{y}; \mathbf{x}', \mathbf{y}') = \langle \psi_{\kappa}^{\dagger}(\mathbf{x}') \psi_{\lambda}^{\dagger}(\mathbf{y}') \psi_{\nu}(\mathbf{y}) \psi_{\mu}(\mathbf{x}) \rangle \quad (86)$$

by [45]:

$$N_b = \frac{1}{2} \sum_{\mu\nu\kappa\lambda} \int d\mathbf{r} d\mathbf{r}' d\mathbf{R} [\phi_b^{(\mu\nu)}(\mathbf{r})]^* G_{\mu\nu\kappa\lambda}^{(2)}\left(\mathbf{R} + \frac{\mathbf{r}}{2}, \mathbf{R} - \frac{\mathbf{r}}{2}; \mathbf{R} + \frac{\mathbf{r}'}{2}, \mathbf{R} - \frac{\mathbf{r}'}{2}\right) \phi_b^{(\kappa\lambda)}(\mathbf{r}'). \quad (87)$$

Here the spatial integration variables can be interpreted in terms of two-body centre of mass and relative coordinates $\mathbf{R} = (\mathbf{x} + \mathbf{y})/2$ and $\mathbf{r} = \mathbf{x} - \mathbf{y}$, respectively. The number of correlated pairs of atoms in the scattering continuum can be deduced from the two-body correlation function in a similar way [45] with the multichannel bound state wave function replaced by the continuum states. We note that Eq. (87) neither

assumes any particular class of many-body states nor any approximation to the many-body Schrödinger equation. By expanding the two-body correlation function in Eq. (87) into cumulants and truncating the expansion in accordance with the first order cumulant approach, the density of bound molecules can be represented in terms of a molecular mean field [45]:

$$\Psi_b(\mathbf{R}, t) = \frac{1}{\sqrt{2}} \sum_{\mu\nu} \int d\mathbf{r} [\phi_b^{(\mu\nu)}(\mathbf{r})]^* \left[\Phi_{\mu\nu}(\mathbf{R}, \mathbf{r}, t) + \Psi_{\mu}\left(\mathbf{R} + \frac{\mathbf{r}}{2}, t\right) \Psi_{\nu}\left(\mathbf{R} - \frac{\mathbf{r}}{2}, t\right) \right]. \quad (88)$$

Here we have introduced the centre of mass and relative coordinates \mathbf{R} and \mathbf{r} and represented the pair function in terms of these variables. The molecular mean field determines the density of diatomic molecules in the state ϕ_b by $n_b(\mathbf{R}, t) = |\Psi_b(\mathbf{R}, t)|^2$. The molecular mean field as well as the fraction of pairs of correlated atoms in the scattering continuum are determined completely by the solution of the coupled equations (81) and (82).

2. Two channel approach

The general form of the two-body Hamiltonian in Eq. (83) with a realistic potential matrix allows us to describe the bi-

nary collision physics over a wide range of energies and magnetic field strengths, as indicated in Fig. 1. As the present applications involve only the adiabatic association of molecules in the vicinity of the 100 mT Feshbach resonance of ^{87}Rb , we can restrict the asymptotic binary scattering channels to those that we have identified in Section II. We shall thus insert the two channel description of Section II into Eqs. (81) and (82) and perform the pole approximation of Subsection II B. The relevant potentials then involve the background scattering potential $V_{bg}(r)$ and the off diagonal matrix element $W(r)$ between the open channel and the closed channel strongly coupled to it. In accordance with the pole approximation, the only configuration of the atoms in this closed channel is the diatomic resonance state $\phi_{res}(r)$. Consequently, the atomic mean

field is restricted to its component in the ($F = 1, m_F = +1$) state, which we shall denote simply by $\Psi(\mathbf{x}, t)$. According to

Eq. (81), the associated mean field dynamic equation is then given by

$$i\hbar \frac{\partial}{\partial t} \Psi(\mathbf{x}, t) = \left[-\frac{\hbar^2}{2m} \nabla^2 + V_{\text{trap}}(\mathbf{x}) \right] \Psi(\mathbf{x}, t) + \int d\mathbf{y} \Psi^*(\mathbf{y}, t) \left(W(|\mathbf{x} - \mathbf{y}|) \Phi_{\text{cl}}(\mathbf{x}, \mathbf{y}, t) + V_{\text{bg}}(|\mathbf{x} - \mathbf{y}|) \left[\Phi_{\text{bg}}(\mathbf{x}, \mathbf{y}, t) + \Psi(\mathbf{x}, t) \Psi(\mathbf{y}, t) \right] \right) \quad (89)$$

The pair function has a component in the open channel and in the closed channel strongly coupled to it. In accordance with

Eq. (82), their coupled dynamic equations read:

$$i\hbar \frac{\partial}{\partial t} \begin{pmatrix} \Phi_{\text{bg}}(\mathbf{x}, \mathbf{y}, t) \\ \Phi_{\text{cl}}(\mathbf{x}, \mathbf{y}, t) \end{pmatrix} = H_{\text{trap}}^{2\text{B}}(t) \begin{pmatrix} \Phi_{\text{bg}}(\mathbf{x}, \mathbf{y}, t) \\ \Phi_{\text{cl}}(\mathbf{x}, \mathbf{y}, t) \end{pmatrix} + \begin{pmatrix} V_{\text{bg}}(|\mathbf{x} - \mathbf{y}|) \\ W(|\mathbf{x} - \mathbf{y}|) \end{pmatrix} \Psi(\mathbf{x}, t) \Psi(\mathbf{y}, t). \quad (90)$$

Here $H_{\text{trap}}^{2\text{B}}(t)$ is the general two channel two-body Hamiltonian [cf. Eq. (2)] that includes the centre of mass kinetic energy of a pair of atoms as well as the confining harmonic potential of the atom trap. In the two channel formulation of the first order microscopic quantum dynamics approach, Eqs. (89) and (90) completely determine the dynamics of the coherent atomic condensate and the fraction of correlated pairs of atoms.

For the purpose of numerical convenience, we shall solve the inhomogeneous linear Schrödinger equation (90) formally in terms of the complete two-body time evolution operator

$U_{\text{trap}}^{2\text{B}}(t, \tau)$ [cf. Eq. (44)] that accounts for the centre of mass motion of the atoms and for the confining trap potential. We shall then insert the solution into the mean field equation (89) to eliminate the pair function. We shall assume that at the initial time t_i at the start of the ramp the gas is well described by a dilute zero temperature Bose-Einstein condensate, so that initial two-body correlations are negligible. The resulting dynamic equation for the atomic mean field can then be expressed in terms of the time dependent two-body transition matrix

$$T_{\text{trap}}^{2\text{B}}(t, \tau) = \langle \text{bg} | \left[V(t) \delta(t - \tau) + \frac{1}{i\hbar} \theta(t - \tau) V(t) U_{\text{trap}}^{2\text{B}}(t, \tau) V(\tau) \right] | \text{bg} \rangle, \quad (91)$$

which involves the potential matrix

$$V(t) = \begin{pmatrix} V_{\text{bg}} & W \\ W & V_{\text{cl}}(B(t)) \end{pmatrix} \quad (92)$$

and the two-body time evolution operator $U_{\text{trap}}^{2\text{B}}(t, \tau)$. Here $|\text{bg}\rangle$ denotes the internal state of a pair of atoms in the asymptotic open scattering channel, and $\theta(t - \tau)$ is the step function, which

yields unity at $t > \tau$ and zero elsewhere. A short calculation applying the methods derived in Refs. [26, 45] then shows that the elimination of the pair function in Eq. (89) leads to a closed dynamic equation for the atomic mean field. Expressed in terms of the two-body transition matrix in Eq. (91), this is given by:

$$i\hbar \frac{\partial}{\partial t} \Psi(\mathbf{x}, t) = \left[-\frac{\hbar^2}{2m} \nabla^2 + V_{\text{trap}}(\mathbf{x}) \right] \Psi(\mathbf{x}, t) + \int_{t_i}^{\infty} d\tau \int d\mathbf{y} d\mathbf{x}' d\mathbf{y}' \Psi^*(\mathbf{y}, t) T_{\text{trap}}^{2\text{B}}(\mathbf{x}, \mathbf{y}, t; \mathbf{x}', \mathbf{y}', \tau) \Psi(\mathbf{x}', \tau) \Psi(\mathbf{y}', \tau). \quad (93)$$

In the case of a harmonic trap potential the two-body transition matrix in Eq. (91) factorises into a centre of mass part and

a contribution from the relative motion of an atom pair. In the

following, we shall assume the confinement of the atom trap to be sufficiently weak and the ramp speeds to be sufficiently high that the time spent within the width of the resonance is much smaller than the trap periods in all spatial directions. The centre of mass motion of a pair of atoms then becomes negligible on this time scale. The explicit form of Eq. (91) also reveals that the time evolution operator of the relative motion of two atoms is evaluated only within the spatial range of the binary interaction potentials, where it is hardly modified by the presence of the atom trap. Consequently, the trap potential can also be neglected in the two-body time evolution operator of the relative motion of an atom pair. Furthermore, as the atomic mean field is slowly varying on the length scales set by the binary interaction potentials, Eq. (93) becomes local in the spatial variables and acquires the form [26, 45]:

$$i\hbar \frac{\partial}{\partial t} \Psi(\mathbf{x}, t) = \left[-\frac{\hbar^2}{2m} \nabla^2 + V_{\text{trap}}(\mathbf{x}) \right] \Psi(\mathbf{x}, t) - \Psi^*(\mathbf{x}, t) \int_{t_i}^{\infty} d\tau \Psi^2(\mathbf{x}, \tau) \frac{\partial}{\partial \tau} h(t, \tau). \quad (94)$$

Here we have introduced the coupling function

$$h(t, \tau) = \theta(t - \tau) (2\pi\hbar)^3 \langle 0, \text{bg} | V(t) U_{2B}(t, \tau) | 0, \text{bg} \rangle, \quad (95)$$

which depends on the time evolution operator $U_{2B}(t, \tau)$ associated with the relative motion of an atom pair in free space, while $|0, \text{bg}\rangle$ denotes the zero momentum plane wave state of the relative motion of two atoms in the asymptotic open scattering channel.

3. Atomic condensate fraction

As we have shown in Subsections IIC, IID and IIE, the two-body time evolution of the main physical observables of interest in the adiabatic association of molecules is largely independent of the details of the implementation of the two-body Hamiltonian. The main requirement is that the two-body Hamiltonian properly accounts for the magnetic field dependence of the scattering length and the near resonant binding energy of the highest excited vibrational bound state. The differences between a single and a two channel treatment (cf. Subsection IID) in the dynamics of the atomic mean field in Eq. (94) are marginal (cf., also, Ref. [54]). The following calculations have, therefore, been performed with a single channel two-body Hamiltonian as introduced in Ref. [45] and described in the appendix. In the course of our studies, we have solved Eq. (94) for a variety of linear ramps of the magnetic field strength across the 100 mT Feshbach resonance of ^{87}Rb in spherically as well as cylindrically symmetric harmonic atom traps. Figure 8 shows the time evolution of the number of condensate atoms $N_c(t) = \int d\mathbf{x} |\Psi(\mathbf{x}, t)|^2$ for linear downward ramps with a ramp speed of 0.1 mT/ms in spherically symmetric atom traps with the frequencies $\nu_{\text{ho}} = 100$ Hz and $\nu_{\text{ho}} = 10$ Hz. The atomic mean field at the initial time $t_i = 0$ has been chosen in each calculation as the ground state of the Gross-Pitaevskii equation that corresponds to a dilute zero temperature Bose-Einstein condensate with $N = 50000$

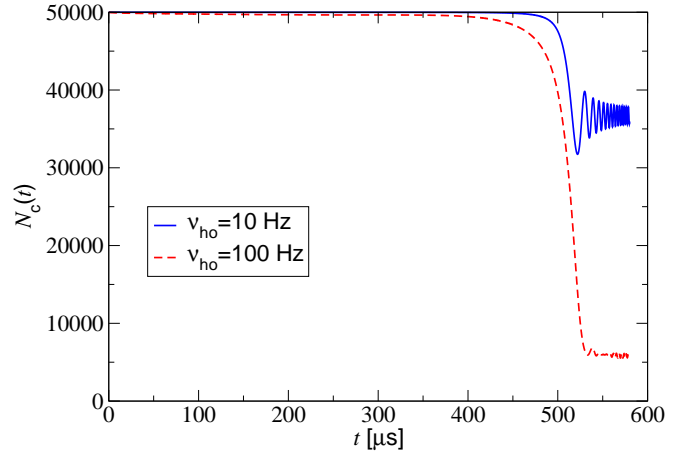


FIG. 8: The time evolution of the condensate fraction ($N_c(t) = \int d\mathbf{x} |\Psi(\mathbf{x}, t)|^2$) for a linear downward ramp of the magnetic field strength across the 100 mT Feshbach resonance of ^{87}Rb . The solid curve shows a calculation for a weakly confining spherical atom trap with the frequency $\nu_{\text{ho}} = 10$ Hz, while the dashed curve corresponds to a comparatively strongly confining ($\nu_{\text{ho}} = 100$ Hz) spherical atom trap. The ramp speed in both calculations is 0.1 mT/ms and the initial number of condensate atoms is $N = 50000$. The time at which the magnetic field strength crosses the resonance position is $t = 500 \mu\text{s}$.

atoms and a scattering length of $a_{\text{bg}} = 100 a_{\text{Bohr}}$. Figure 8 reveals that the loss of condensate atoms mainly occurs during the passage across the Feshbach resonance. In accordance with the higher local density, the losses of condensate atoms are more pronounced in the comparatively strongly confining 100 Hz atom trap. The pronounced oscillations immediately after the passage across the resonance ($t > 500 \mu\text{s}$) indicate a rapid exchange between the condensed and the noncondensed phases of the gas. Exchange on these short time scales suggests that the crossing of a Feshbach resonance drives the gas into a highly excited nonequilibrium state.

Figure 9 shows snapshots of the condensate density $n_c(\mathbf{x}, t) = |\Psi(\mathbf{x}, t)|^2$ as a function of the radial coordinate $r = |\mathbf{x}|$ for the ramps and trap parameters in Fig. 8 at the final time $t_f = 580 \mu\text{s}$. The pronounced spatial variations of the remnant condensate density indicate the simultaneous occupation of many collective energy modes. We note that these highly occupied excited modes are described by a coherent classical mean field and are therefore distinguished from the pairs of correlated atoms in the initially unoccupied scattering continuum. In accordance with Eq. (84), correlated pairs of atoms, as described by the pair function $\Phi(t)$, constitute the density of the noncondensed fraction.

4. Noncondensed fraction

We shall study in the following how the final noncondensed fraction of the gas is distributed among the bound and free energy states of an atom pair. We shall focus on linear downward ramps of the magnetic field strength across the 100 mT Feshbach resonance of ^{87}Rb . Given the solution of the dynamic

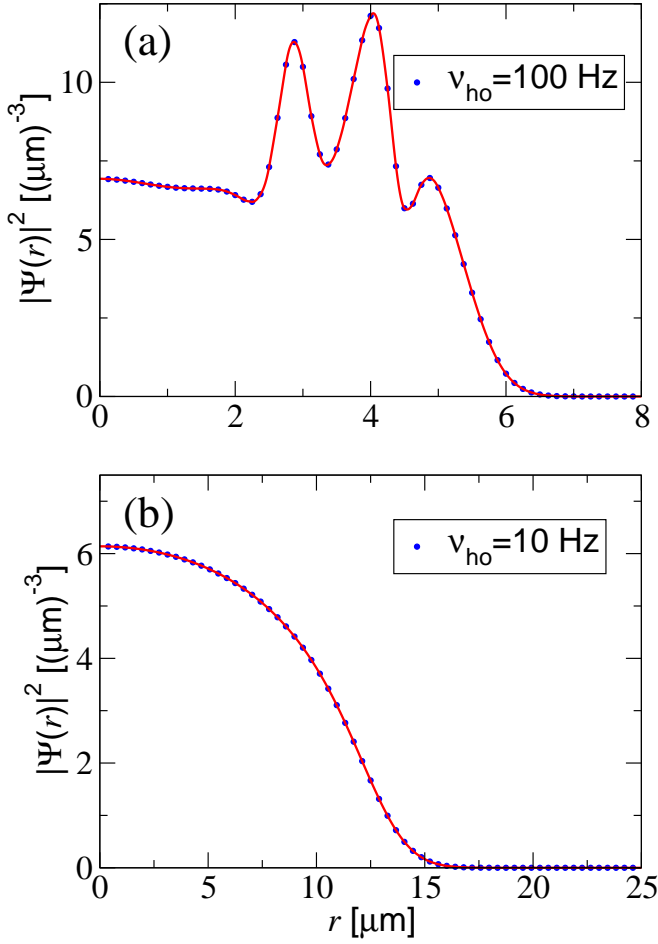


FIG. 9: Snapshots of the remnant condensate density after the crossing of the 100 mT Feshbach resonance of ^{87}Rb in spherically symmetric atom traps with the frequencies $\nu_{\text{ho}} = 100$ Hz (a) and $\nu_{\text{ho}} = 10$ Hz (b). The densities correspond to the calculations in Fig. 8 at the final time of the ramps.

equation (94) for the atomic mean field, the pair function $\Phi(t)$ is determined completely by the inhomogeneous linear two-body Schrödinger equation (90). We shall assume that the trap is switched off immediately after the ramp so that the gas expands freely in space. Inserting the complete set of two-body energy states (cf. Subsection II B) at the final magnetic field strength B_f into Eq. (84), and integrating with respect to the centre of mass coordinate $\mathbf{R} = (\mathbf{x} + \mathbf{y})/2$ yields the number of noncondensate atoms [45]:

$$N_{\text{nc}} = \int d\mathbf{R} \int d\mathbf{p} \left| \langle \mathbf{R}, \phi_{\text{p}}(B_f) | \Phi(t_f) \rangle \right|^2 + \int d\mathbf{R} \left| \langle \mathbf{R}, \phi_{\text{b}}(B_f) | \Phi(t_f) \rangle \right|^2. \quad (96)$$

Here we have presupposed that only the energetically accessible highest excited vibrational multichannel bound state $\phi_{\text{b}}(B_f)$ on the low field side of the Feshbach resonance (cf. Subsection II C) will be populated in a downward ramp. We shall assume furthermore that the final magnetic field strength is sufficiently far from the Feshbach resonance that

the gas is weakly interacting; i.e. $n_{\text{peak}}[a(B_f)]^3 \ll 1$, where n_{peak} is the peak density of the gas, and $a(B_f)$ is the final scattering length. The second, factorised contribution to the molecular mean field on the right hand side of Eq. (88) can then be neglected [45]. Consequently, the bound state contribution to the noncondensed density on the right hand side of Eq. (96) determines the number of atoms associated to molecules. The contribution of the continuum part of the two-body energy spectrum yields the burst fraction, composed of correlated atoms with a comparatively high relative momentum $|\mathbf{p}|$ in initially unoccupied modes [45]. According to Eqs. (85) and (96), the number of condensate atoms, atoms associated to molecules and burst atoms then add up to the total number of atoms. We note that Eqs. (85) and (96) are also applicable in the small region of magnetic field strengths in the close vicinity of the Feshbach resonance, in which the gas becomes strongly interacting. The dilute gas parameter $n_{\text{peak}}[a(B)]^3$ is then on the order of unity or larger. Under these conditions, however, a separation of the gas into bound and free atoms is physically meaningless [53, 58].

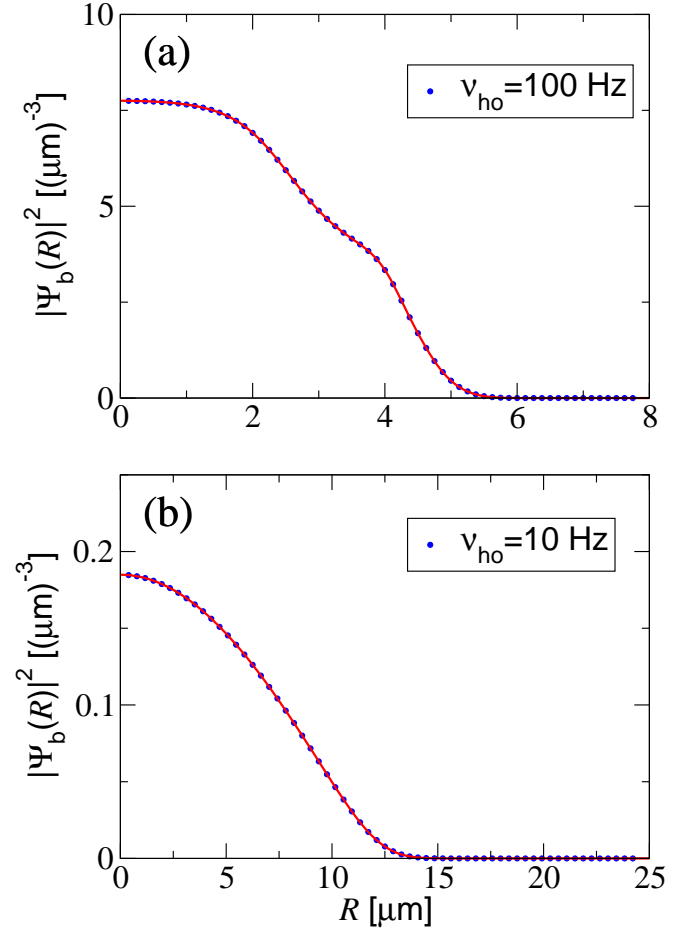


FIG. 10: Density of $^{87}\text{Rb}_2$ molecules in the highest excited vibrational bound state after the crossing of the 100 mT Feshbach resonance in spherically symmetric atoms traps with the frequencies $\nu_{\text{ho}} = 100$ Hz (a) and $\nu_{\text{ho}} = 10$ Hz (b). The molecular densities correspond to the calculations in Fig. 8 at the final time of the ramps.

Figure 10 shows the densities of $^{87}\text{Rb}_2$ molecules in the highest excited vibrational molecular bound state at the final magnetic field strength of the linear downward ramps across the 100 mT Feshbach resonance, which are described in Fig. 8. The densities have been obtained from the molecular mean field $\Psi_b(\mathbf{R}, t_f)$ in Eq. (88) through $n_b(\mathbf{R}, t_f) = |\Psi_b(\mathbf{R}, t_f)|^2$ with the bound state wave function $\phi_b(B_f)$ at the final magnetic field strength B_f of the ramps. The spatial extent of the molecular clouds roughly corresponds to the size of the remnant condensate densities in Fig. 9. In accordance with the higher local densities, the density of molecules in the tight 100 Hz atom trap is higher than in the 10 Hz trap.

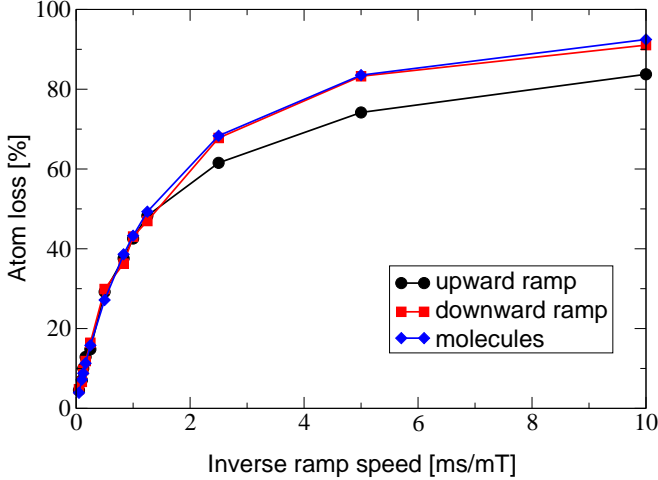


FIG. 11: The relative loss of condensate atoms $[N_c(t_i) - N_c(t_f)]/N_c(t_i)$ in linear upward ramps (circles) as well as downward ramps (squares) of the magnetic field strength across the 100 mT Feshbach resonance of ^{87}Rb as a function of the inverse ramp speed. The upward ramps transfer the condensate atoms into correlated pairs of atoms in initially unoccupied excited states, while the downward ramps adiabatically associate a substantial fraction of the condensate to bound molecules in the highest excited vibrational state. The diamonds indicate the relative number $2N_b(t_f)/N_c(t_i)$ of atoms associated to molecules in the downward ramps. The calculations were performed for a cylindrical atom trap with the axial (radial) frequencies of $\nu_{\text{axial}} = 116$ Hz ($\nu_{\text{radial}} = 75$ Hz) and $N = 140000$ atoms. The small deviations in the calculated loss data of the remnant atomic condensate (filled circles) from an entirely smooth curve are due to rapid oscillations in the atomic condensate fraction after the passage of the Feshbach resonance (see Fig. 8), which have not entirely decayed at the final times that we have chosen for the different inverse ramp speeds.

Figure 11 shows systematic studies of the dependence of the molecular production, after downward ramps of the magnetic field strength across the 100 mT Feshbach resonance of ^{87}Rb , on the inverse ramp speed. The calculations have been performed on the basis of the dynamic equation (94) for the atomic mean field. In these calculations we have chosen the potential of a comparatively tight cylindrically symmetric optical atom trap with axial and radial frequencies (see Fig. 11) that resemble those in current experiments on the production of ultracold $^{87}\text{Rb}_2$ molecules in Oxford [59]. The initial state has been chosen as the ground state of the Gross-Pitaevskii

equation with $N_c(t_i) = 140000$ atoms and a scattering length of $a_{\text{bg}} = 100 a_{\text{Bohr}}$. The squares in Fig. 11 indicate the relative loss of condensate atoms $[N_c(t_i) - N_c(t_f)]/N_c(t_i)$ in the downward ramps, where $N_c(t) = \int d\mathbf{x} |\Psi(\mathbf{x}, t)|^2$ is the number of condensate atoms at time t . As expected from the two-body considerations in Subsection IIE, the loss curve is a monotonic function of the inverse ramp speed and saturates when the remnant condensate is completely depleted. The number of atoms associated to diatomic molecules in the highest excited vibrational bound state $\phi_b(B_f)$ is given by $2N_b(t_f) = 2 \int d\mathbf{R} |\Psi_b(\mathbf{R}, t_f)|^2$, where $\Psi_b(\mathbf{R}, t_f)$ is the molecular mean field in Eq. (88). The dependence of the relative molecular association efficiency $2N_b(t_f)/N_c(t_i)$ on the inverse ramp speed in the downward ramps is indicated by the diamonds in Fig. 11 and follows the same monotonic trend as the loss curve of condensate atoms in the downward ramps (squares). The quantitative agreement between both curves shows that the missing fraction of condensate atoms is transferred into diatomic molecules in the highest excited multi-channel vibrational bound state. The excitation of atom pairs in continuum energy modes is suppressed. The rapid loss of condensate atoms, however, leads to an overall heating of the atomic cloud due to the excitation of collective energy modes (see Fig. 9).

The circles in Fig. 11 indicate predictions of the total loss of condensate atoms in upward ramps of the magnetic field strength across the 100 mT Feshbach resonance of ^{87}Rb . The initial state of the gas as well as the confining atom trap in these calculations are the same as in the downward ramps. The final magnetic field strength B_f , after the passage across the resonance in an upward ramp, is on the high field side of the resonance position. Figure 2 reveals that there is no energetically accessible bound state at the magnetic field strength B_f . Consequently, atoms lost from the condensate are entirely transferred into the burst fraction. Figure 11 shows that despite an overall agreement in the monotonic behaviour of the condensate loss with increasing inverse ramp speeds, there is a small difference in the saturation region between the curves for the different ramp directions. This small deviation between the curves would be absent in the two-body description of Section II and may indicate phenomena related to the coherent nature of the gas.

B. Two level mean field approach

One of the most common approaches to the association of molecules in dilute Bose-Einstein condensates is based on a model many-body Hamiltonian that describes atoms and molecules in terms of separate quantum fields. The coupling between these quantum fields leads to an exchange between the different species. This exchange then serves as a model for the molecular production.

1. Markov approximation to the first order microscopic quantum dynamics approach

In order to reveal the physical meaning of the molecular quantum field and its relation to the microscopic quantum dynamics approach of Subsection III A, we shall derive the mean field equations associated with the two component model Hamiltonian on the basis of the first order coupled dynamic equations (89) and (90) that determine the atomic mean field and the pair function. We shall represent the pair function in terms of the centre of mass and relative coordinates \mathbf{R} and \mathbf{r} , respectively. In accordance with the pole approximation of Subsection II B, the closed channel part of the pair function can be factorised into the resonance state $\phi_{\text{res}}(r)$ and a centre of mass wave function:

$$\Phi_{\text{cl}}(\mathbf{R}, \mathbf{r}, t) = \sqrt{2}\phi_{\text{res}}(r)\Psi_{\text{res}}(\mathbf{R}, t). \quad (97)$$

$$\begin{aligned} \Phi_{\text{bg}}(\mathbf{R}, \mathbf{r}, t) = & \int d\mathbf{R}' d\mathbf{r}' \langle \mathbf{R}, \mathbf{r} | U_{\text{trap}}^{\text{bg}}(t - t_i) | \mathbf{R}', \mathbf{r}' \rangle \Phi_{\text{bg}}(\mathbf{R}', \mathbf{r}', t_i) \\ & + \frac{1}{i\hbar} \int_{t_i}^t d\tau \int d\mathbf{R}' d\mathbf{r}' \langle \mathbf{R}, \mathbf{r} | U_{\text{trap}}^{\text{bg}}(t - \tau) V_{\text{bg}} | \mathbf{R}', \mathbf{r}' \rangle \Psi(\mathbf{R}' + \mathbf{r}'/2, \tau) \Psi(\mathbf{R}' - \mathbf{r}'/2, \tau) \\ & + \frac{1}{i\hbar} \int_{t_i}^t d\tau \int d\mathbf{R}' \langle \mathbf{R}, \mathbf{r} | U_{\text{trap}}^{\text{bg}}(t - \tau) W | \mathbf{R}', \phi_{\text{res}} \rangle \sqrt{2}\Psi_{\text{res}}(\mathbf{R}', \tau). \end{aligned} \quad (98)$$

We note that $U_{\text{trap}}^{\text{bg}}(t - \tau)$ includes the centre of mass and the relative motion of two atoms as well as the confining potential of the atom trap.

To obtain the mean field equations for $\Psi(\mathbf{x}, t)$ and the centre of mass wave function $\Psi_{\text{res}}(\mathbf{R}, t)$ in Eq. (97), we shall insert Eq. (98) into Eqs. (89) and (90) and perform the Markov approximation. The Markov approximation relies upon the assumption that the main contribution to the time integrals in Eq. (98) stems from a small region near $\tau = t$, in which the variation of the functions $\Psi(\mathbf{R}' + \mathbf{r}'/2, \tau)$, $\Psi(\mathbf{R}' - \mathbf{r}'/2, \tau)$ and $\Psi_{\text{res}}(\mathbf{R}', \tau)$ is negligible. Under this assumption, the functions can be evaluated at $\tau = t$. A similar argument applies to the spatial variation of $\Psi(\mathbf{R}' + \mathbf{r}'/2, \tau)$, $\Psi(\mathbf{R}' - \mathbf{r}'/2, \tau)$ and $\Psi_{\text{res}}(\mathbf{R}', \tau)$ and leads to the replacements $\mathbf{R}' \rightarrow \mathbf{R}$ and $\mathbf{r}' \rightarrow 0$ in these functions. The subsequent formal procedure to derive the mean field equations is analogous to the derivation of the Gross-Pitaevskii equation in Ref. [26] and involves neglecting the initial pair function $\Phi_{\text{bg}}(\mathbf{R}', \mathbf{r}', t_i)$ and the centre of mass motion as well as the confining potential of the atom trap in the time evolution operator $U_{\text{trap}}^{\text{bg}}(t - \tau)$. A short calculation then yields the coupled equations

$$\begin{aligned} i\hbar \frac{\partial}{\partial t} \Psi(\mathbf{x}, t) = & \left[-\frac{\hbar^2}{2m} \nabla^2 + \frac{m}{2} \omega_{\text{ho}}^2 |\mathbf{x}|^2 \right] \Psi(\mathbf{x}, t) \\ & + g_{\text{bg}} |\Psi(\mathbf{x}, t)|^2 \Psi(\mathbf{x}, t) \\ & + g_{\text{res}} \Psi^*(\mathbf{x}, t) \sqrt{2} \Psi_{\text{res}}(\mathbf{x}, t) \end{aligned} \quad (99)$$

In the following derivation we shall show that the centre of mass wave function $\Psi_{\text{res}}(\mathbf{R}, t)$ is identical to the mean field associated with the molecular quantum field in the two component model Hamiltonian. To this end we shall proceed in a way similar to the derivation of the dynamic equation (94) for the atomic mean field in Subsection III A, except that we shall eliminate only the component $\Phi_{\text{bg}}(\mathbf{R}, \mathbf{r}, t)$ of the pair function in the open channel from Eqs. (89) and (90). The formal solution of the dynamic equation for $\Phi_{\text{bg}}(\mathbf{R}, \mathbf{r}, t)$ [i.e. the first component of Eq. (90)] can be expressed in terms of the two-body time evolution operator $U_{\text{trap}}^{\text{bg}}(t - \tau)$ that corresponds to the stationary diagonal element $\langle \text{bg} | H_{2\text{B}} | \text{bg} \rangle$ of the full two-body Hamiltonian matrix $H_{2\text{B}}(t)$ [cf. Eq. (90)] in the open channel:

for the atomic mean field, and

$$\begin{aligned} i\hbar \frac{\partial}{\partial t} \Psi_{\text{res}}(\mathbf{R}, t) = & \left[-\frac{\hbar^2}{4m} \nabla^2 + \frac{2m}{2} \omega_{\text{ho}}^2 |\mathbf{R}|^2 \right] \Psi_{\text{res}}(\mathbf{R}, t) \\ & + \left[\frac{dE_{\text{res}}}{dB}(B_{\text{res}}) \right] [B(t) - B_0] \Psi_{\text{res}}(\mathbf{R}, t) \\ & + \frac{1}{\sqrt{2}} g_{\text{res}} \Psi^2(\mathbf{R}, t) \end{aligned} \quad (100)$$

for the molecular mean field [46]. Here we have assumed the optical atom trap to be spherically symmetric. The coupling constants g_{bg} and g_{res} can be obtained by performing the spatial as well as the time integrations in Eq. (98) in the limit $t - t_i \rightarrow \infty$. This yields (cf., also, Ref. [26]):

$$g_{\text{bg}} = \frac{4\pi\hbar^2}{m} a_{\text{bg}} \quad (101)$$

$$g_{\text{res}} = (2\pi\hbar)^{3/2} \langle \phi_{\text{res}} | W | \phi_0^{(+)} \rangle. \quad (102)$$

Here a_{bg} is the background scattering length and $\phi_0^{(+)}(\mathbf{r})$ is the zero energy wave function associated with the background scattering (cf. Eq. (8)). We note that the off diagonal coupling constant g_{res} is defined only up to a global phase and we shall, therefore, choose it to be real. In accordance with Eq. (25), g_{res} is then determined by the resonance width (ΔB) , the background scattering length a_{bg} and the slope of the resonance $\left[\frac{dE_{\text{res}}}{dB}(B_{\text{res}}) \right]$. The mean field equations (99) and (100)

as well as the coupling constants in Eqs. (101) and (102) are analogous to those that have been applied, for instance, in Ref. [61] to describe the atom loss in ramps of the magnetic field strength across Feshbach resonances in ^{23}Na . In the applications of the mean field equations (99) and (100), the densities $n_c(\mathbf{x}, t) = |\Psi(\mathbf{x}, t)|^2$ and $n_{\text{res}}(\mathbf{R}, t) = |\Psi_{\text{res}}(\mathbf{R}, t)|^2$ are usually interpreted as atomic and molecular condensate densities, respectively.

2. Two component model Hamiltonian

Equations (99) and (100) can be derived formally as equations of motion for the mean fields

$$\Psi(\mathbf{x}, t) = \langle \psi(\mathbf{x}) \rangle_t \quad (103)$$

$$\Psi_{\text{res}}(\mathbf{R}, t) = \langle \psi_{\text{res}}(\mathbf{R}) \rangle_t \quad (104)$$

in the Hartree approximation. The corresponding two component model Hamiltonian is given by:

$$\begin{aligned} H = & \int d\mathbf{x} \psi^\dagger(\mathbf{x}) \left[-\frac{\hbar^2}{2m} \nabla^2 + \frac{m}{2} \omega_{\text{ho}}^2 |\mathbf{x}|^2 \right] \psi(\mathbf{x}) \\ & + \int d\mathbf{R} \psi_{\text{res}}^\dagger(\mathbf{R}) \left[-\frac{\hbar^2}{4m} \nabla^2 + \frac{2m}{2} \omega_{\text{ho}}^2 |\mathbf{R}|^2 \right] \psi_{\text{res}}(\mathbf{R}) \\ & + \int d\mathbf{R} \psi_{\text{res}}^\dagger(\mathbf{R}) \left[\frac{dE_{\text{res}}}{dB}(B_{\text{res}}) \right] [B(t) - B_0] \psi_{\text{res}}(\mathbf{R}) \\ & + \frac{1}{2} g_{\text{bg}} \int d\mathbf{x} \psi^\dagger(\mathbf{x}) \psi^\dagger(\mathbf{x}) \psi(\mathbf{x}) \psi(\mathbf{x}) \\ & + \frac{1}{\sqrt{2}} g_{\text{res}} \int d\mathbf{x} \left[\psi_{\text{res}}^\dagger(\mathbf{x}) \psi(\mathbf{x}) \psi(\mathbf{x}) + \text{h.c.} \right]. \end{aligned} \quad (105)$$

Here the field operators $\psi(\mathbf{x})$ and $\psi_{\text{res}}(\mathbf{R})$ fulfil the usual Bose commutation relations and commute among the different species:

$$[\psi(\mathbf{x}), \psi_{\text{res}}(\mathbf{R})] = 0 \quad (106)$$

$$[\psi(\mathbf{x}), \psi_{\text{res}}^\dagger(\mathbf{R})] = 0. \quad (107)$$

3. Deficits of the two level mean field approach

Despite its common use in studies of molecular association in dilute Bose-Einstein condensates, the two level mean field model in Eqs. (99) and (100) and its common interpretation are subject to two serious deficits. First, in the derivation of the mean field equations we have shown that the mean field $\Psi_{\text{res}}(\mathbf{R}, t)$ is associated with a pair of atoms in the closed channel resonance state $\phi_{\text{res}}(r)$ [see Eq. (97)]. Figure 3 clearly reveals that, in general, such an atom pair cannot be associated with a molecular bound state because in the close vicinity of the 100 mT Feshbach resonance of ^{87}Rb , as well as asymptotically far from it, the wave function of the highest excited vibrational bound state is dominated by its component in the open channel [62].

The interpretation of $N_{\text{res}}(t) = \int d\mathbf{R} |\Psi_{\text{res}}(\mathbf{R}, t)|^2$ in terms of the population in the resonance state (as opposed to the number of bound molecules) is a direct consequence of the commutation relation in Eq. (107) and of the form of the Hamiltonian in Eq. (105), rather than an artifact of the derivation of the mean field equations (99) and (100). In fact, according to Eq. (107), a localised pair of atoms created from the vacuum state $|\text{vac}\rangle$ by the field operator $\psi_{\text{res}}^\dagger(\mathbf{R})$ is always orthogonal to the localised state of any atom pair created by $\psi^\dagger(\mathbf{y})\psi^\dagger(\mathbf{x})$ in the open channel; i.e.

$$\langle \text{vac} | \psi(\mathbf{x}) \psi(\mathbf{y}) \psi_{\text{res}}^\dagger(\mathbf{R}) | \text{vac} \rangle = 0. \quad (108)$$

The two states of the atom pairs, therefore, correspond to different asymptotic scattering channels. It can also be verified from the Hamiltonian in Eq. (105) that any physical two-body state associated with $\psi_{\text{res}}^\dagger(\mathbf{R})|\text{vac}\rangle$ is not stationary with respect to the time evolution in the relative motion of the atom pairs. The off diagonal coupling in Eq. (105) leads to a decay into the open channel, which is determined by the coupling constant g_{res} . The energy $E_{\text{res}}(B) = \left[\frac{dE_{\text{res}}}{dB}(B_{\text{res}}) \right] (B - B_0)$, which can be associated with $\psi_{\text{res}}^\dagger(\mathbf{R})|\text{vac}\rangle$, is linear in the magnetic field strength and corresponds to the resonance state rather than to the bound molecular states (cf. Fig. 2). The off diagonal coupling constant g_{res} then determines the corresponding decay width.

Although it seems conceivable to measure the closed channel resonance state population $N_{\text{res}}(t) = \int d\mathbf{R} |\Psi_{\text{res}}(\mathbf{R}, t)|^2$, several present day experiments on molecular association in Bose-Einstein condensates have clearly revealed the multi-channel nature of the bound states. The experiments in Refs. [7, 8], for instance, have determined the near resonant universal form $E_b(B) = -\hbar^2 / \{m[a(B)]^2\}$ of the binding energy in Eq. (39), corresponding to a bound state wave function of the universal form of Eq. (40), which is dominated by its component in the asymptotic open channel (cf., also, Fig. 4). The experiment in Ref. [10] has determined the change of the magnetic moment of the molecular bound states in dependence on the magnetic field strength B , which is a consequence of the nonlinear dependence of the binding energy on B (see Fig. 2). The magnetic moment of the resonance state, however, is independent of B . These experiments clearly reveal that the number of bound molecules in Eq. (87) is the relevant physical quantity rather than the resonance state population.

The second major deficit of the mean field equations (99) and (100) in the description of the adiabatic association technique is related to their two level nature; the only configurations of two atoms are a pair of condensate atoms and the resonance state. Neither the near resonant diatomic bound states nor the continuum states can be represented solely in terms of these two configurations. In particular, any coupling between the initial atomic condensate and the quasi continuum of states above the dissociation threshold energy of the open channel is ruled out. The two level nature of Eqs. (99) and (100) is a consequence of the application of the Markov approximation to Eqs. (89) and (90). This indicates that the presuppositions leading to the Markov approximation are violated during the passage across a Feshbach resonance. Consequently,

Eqs. (99) and (100) fail quantitatively and even qualitatively in the dynamic description of the near resonant atom-molecule coherence experiments in Refs. [7, 8]. The most striking consequence of their two level nature, however, consists in the insensitivity of Eqs. (99) and (100) with respect to the ramp direction. The approach thus predicts molecular production even for an upward ramp across the 100 mT Feshbach resonance of ^{87}Rb , although there is no energetically accessible diatomic vibrational bound state on the high field side of the resonance (cf. Fig. 2). The reason for this failure is the absence of continuum states that the closed channel resonance state could decay into. The results of Subsection II E suggest, however, that the two level mean field approach may recover the far resonant asymptotic molecular population in a downward ramp of the magnetic field strength across the 100 mT Feshbach resonance of ^{87}Rb .

4. Applications of the two component model Hamiltonian beyond mean field

When applied beyond mean field [63, 64, 65], the model Hamiltonian in Eq. (105) leads to ultraviolet singularities that are related to the energy independence of the coupling constants g_{bg} and g_{res} , i.e. the associated contact potentials crucially lack any spatial extent. The approach in Ref. [63] circumvents this ultraviolet problem in terms of an energy cutoff, which is adjusted in such a way that the Hamiltonian, when applied to only two atoms, recovers the exact binding energy of the highest excited vibrational bound state. This beyond mean field approach has been applied recently to the experiments in Ref. [7]. We expect this approach to give results similar to those of the first order microscopic quantum dynamics approach. It has been pointed out [45, 53, 66, 67, 68], however, that the interpretation in Ref. [63] of the closed channel resonance state population $N_{\text{res}}(t)$ in terms of the number of bound molecules (i.e. the number of undetected atoms in Ref. [7]) is not applicable.

Some approaches [67, 68] have suggested curing this deficit, by multiplying the closed channel resonance state population $N_{\text{res}}(t)$, as determined in Ref. [63], with a magnetic field dependent factor, termed the wave function renormalisation factor, which accounts for the component of the bound state wave function in the asymptotic open scattering channel. A short calculation using Eq. (30) shows that the wave function renormalisation factor is equivalent to the squared normalisation factor

$$\mathcal{N}_b^2 = 1 + \frac{1}{2} \left[\frac{dE_{\text{res}}(B_{\text{res}})}{dB} \right] (\Delta B) \frac{a_{\text{bg}}}{a(B)} \frac{m[a(B)]^2}{\hbar^2} \quad (109)$$

of the two channel bound state wave function in Eq. (29), provided that the magnetic field strength is sufficiently close to the resonance position that the bound state wave function and its binding energy are universal (see Subsection II C). A comparison between the closed channel resonance state population in Ref. [63], revised by multiplication with the right hand side of Eq. (109) (as provided by Ref. [67]), indeed, largely recovers the magnitude of the molecular fractions predicted

by the first order microscopic quantum dynamics approach in Refs. [45, 53]. The revised resonance state population, however, shows unphysical oscillations between the populations of bound and free atoms (cf. Fig. 3 in Ref. [63]), for magnetic field strengths at which the spatial extent of the highest excited vibrational molecular bound state is by far smaller than the mean interatomic distance in the dilute gas. This unphysical behaviour is due to the fact that not only the bound state wave function in Eq. (29), but also the continuum wave functions in Eqs. (16) and (17), have a closed channel resonance state component. As a consequence, there is no *general* relationship between the closed channel resonance state population of a gas and the number of bound molecules.

The general relationship between the number of bound molecules and the two-body correlation function in Eq. (87), however, is applicable also to the approach in Ref. [63]. Equation (87) applies the appropriate quantum mechanical observable, and will therefore automatically determine the measurable fraction of bound molecules in a gas, provided that molecules identified as separate entities are at all a reasonable concept [53].

C. Comparison between different approaches

We have shown in Subsection III A that, during a linear ramp of the magnetic field strength across a Feshbach resonance, the full microscopic quantum dynamics approach can predict a transfer of atoms from the atomic condensate not only to the bound, but also to the continuum part of the two-body energy spectrum. The transfer into the continuum energy states, however, occurred only in upward ramps of the magnetic field strength across the 100 mT Feshbach resonance of ^{87}Rb . The two level configuration interaction approach of Subsection II E restricts the configuration of an atom pair in the open channel to the lowest energetic quasi continuum state of the background scattering in the atom trap, while in the two level mean field model of Subsection III B all atoms in the ($F = 1, m_F = +1$) hyperfine state are described by a coherent mean field. Both two level approaches, therefore, rule out the production of correlated pairs of atoms in the quasi continuum of two-body energy levels from the outset.

Equations (62) and (63) of the configuration interaction approach and the mean field equations (99) and (100) describe the coupling between the atomic condensate and the closed channel resonance state in essentially the same way, except that the phases of the off diagonal coupling terms are different. The spatial configuration of the atomic condensate in the configuration interaction approach, however, is static, while the two level mean field approach allows the trapped atomic condensate to access coherent collective excitations with a high occupancy of the energy modes. Consequently, the configuration interaction approach can, at least to some extent, be interpreted as a local density approximation to the two level mean field model. In accordance with the derivations in Subsection III B, both two level approaches can, therefore, be considered as the Markov approximation to the first order microscopic quantum dynamics approach of Subsection III A.

Our previous considerations have shown that there exists a qualitative agreement between the approaches, at different levels of approximation, with respect to the prediction of molecular formation in linear downward ramps of the magnetic field strength across the 100 mT Feshbach resonance of ^{87}Rb . The description of the microscopic binary collision physics as well as their treatment of the coherent nature of the Bose-Einstein condensate, however, differ considerably among these approaches. In the following, we shall provide quantitative comparisons between their predictions with respect to the molecular production efficiency of the adiabatic association technique. We will study in detail the dependence of the magnitude of the molecular fraction on experimentally accessible parameters.

1. Universal properties of the molecular production efficiency of a linear ramp of the magnetic field strength

In the adiabatic association technique with linear ramps of the magnetic field strength, the ramp speed $\frac{dB}{dt}$ controls the interatomic interactions. Furthermore, the initial number N of atoms can be varied over a wide range in present experiments, and the trap frequencies determine the confining potential of a harmonic atom trap. The atom trap, the number of atoms as well as their binary interactions control the spectrum of coherent collective excitations of a Bose-Einstein condensate. In the following, we shall consider spherically symmetric atom traps with a radial trap frequency that we denote by ν_{ho} .

Figure 12 shows the predicted dependence of the remnant atomic condensate fraction and of the fraction of atoms associated to diatomic molecules in the highest excited vibrational bound state on the inverse speed of linear downward ramps of the magnetic field strength across the 100 mT Feshbach resonance of ^{87}Rb . We have chosen trap frequencies of 100 Hz (a) and of 10 Hz (b) that correspond to a comparatively strongly and a weakly confining harmonic atom trap, respectively. The initial number of $N_c(t_i) = 50000$ condensate atoms is fixed in all calculations. The predictions correspond to the full first order microscopic quantum dynamics approach (MQDA), the nonlinear configuration interaction equations (62) and (63) (CI), the two level mean field equations (99) and (100) (2 level), and the Landau-Zener asymptotic populations in Eqs. (59) and (60) (LZ). The comparison reveals that the approaches predict similar conversion efficiencies with respect to the association of molecules as well as similar remnant condensate fractions. Only the saturation behaviour of the exponential Landau-Zener (LZ) curves [cf. Eqs. (59) and (60)] differs significantly from all other approaches because it corresponds to the asymptotic populations of the linear equations (55) and (56). These results suggest a remarkable insensitivity of the molecular production in linear ramps of the magnetic field strength with respect to both the details of the microscopic binary collision physics and the coherent nature of the Bose-Einstein condensate.

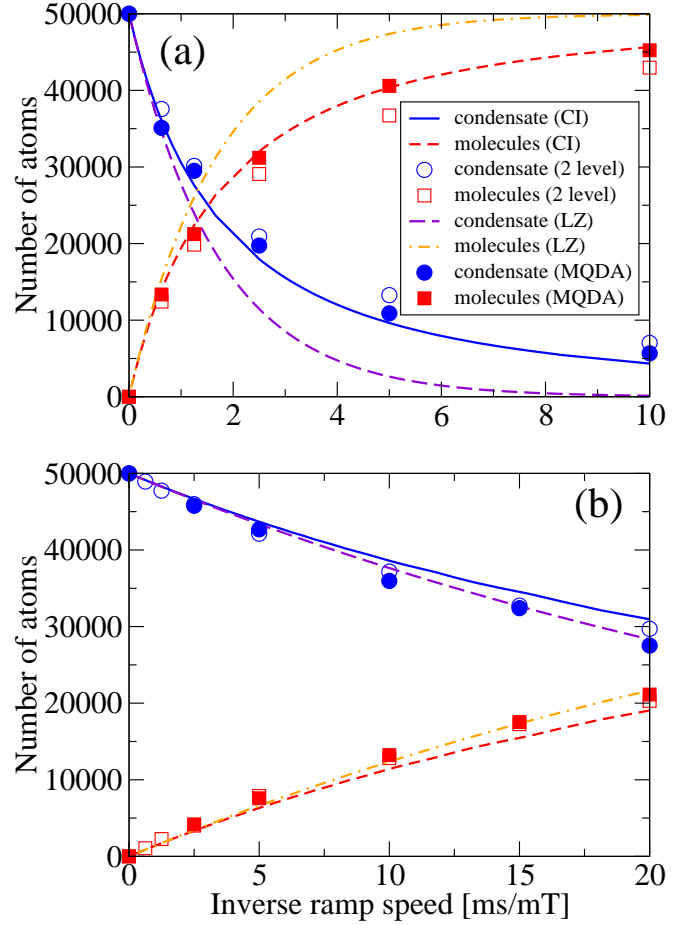


FIG. 12: Predicted remnant condensate fraction and number of atoms associated to diatomic molecules in the highest excited vibrational bound state after a linear downward ramp of the magnetic field strength across the 100 mT Feshbach resonance of ^{87}Rb in dependence on the inverse ramp speed. The initial state of the gas corresponds to a dilute zero temperature Bose-Einstein condensate with a scattering length of $a_{\text{bg}} = 100 a_{\text{Bohr}}$ and $N = 50000$ atoms in spherically symmetric atom traps with the frequencies 100 Hz (a) and 10 Hz (b). The abbreviations in the legend indicate the different approaches applied in the calculations. These approaches contain the first order microscopic quantum dynamics approach (MQDA), the nonlinear configuration interaction equations (62) and (63) (CI), the two level mean field equations (99) and (100) (2 level), and the Landau-Zener asymptotic populations in Eqs. (59) and (60) (LZ). The small deviations in the calculated MQDA data of the remnant atomic condensate (filled circles) from an entirely smooth curve are discussed in Fig. 11.

2. Dependence of the molecular production efficiency on experimentally accessible parameters

We shall now identify the universal physical parameter that controls the molecular production efficiency of the adiabatic association technique. As shown in Subsection II E, the linear Rabi flopping model in Eqs. (55) and (56) leads to an asymptotic fraction of diatomic molecules that can be described by a single parameter, the Landau-Zener coefficient δ_{LZ} . We shall

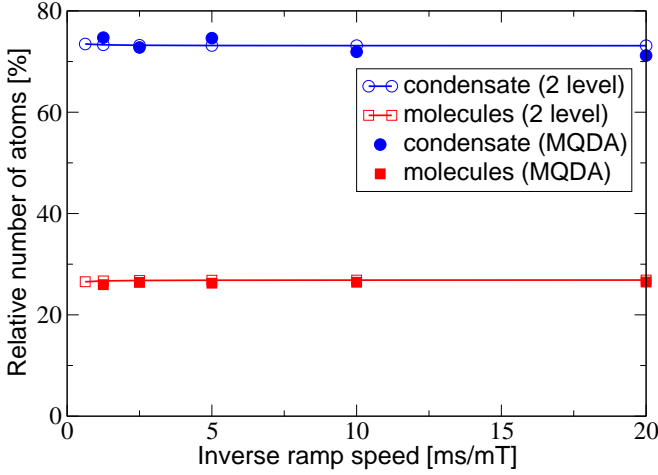


FIG. 13: Predicted proportion of remnant condensate atoms and proportion of atoms associated to diatomic molecules in the highest excited vibrational bound state after a linear downward ramp of the magnetic field strength across the 100 mT Feshbach resonance of ^{87}Rb in dependence on the inverse ramp speed. The atom number and the angular frequency ω_{ho} of the atom trap are adjusted to keep the nonlinearity parameter k_{bg} and the quantity $\omega_{\text{ho}}t_{\text{nat}}$ constant, which also fixes the Landau-Zener parameter δ_{LZ} . The initial states of the gas correspond to a dilute zero temperature Bose-Einstein condensate with a scattering length of $a_{\text{bg}} = 100 a_{\text{Bohr}}$ in spherically symmetric atom traps. In each case the shape of the initial condensate mode is, in units of l_{ho} , identical to that of a dilute Bose-Einstein condensate with 50000 atoms in a spherically symmetric atom trap with a frequency of $\nu_{\text{ho}} = 10$ Hz. The abbreviations in the legend indicate the different approaches applied in the calculations. These approaches contain the first order microscopic quantum dynamics approach (MQDA), and the two level mean field equations (99) and (100) (2 level).

show in the following that also in the nonlinear two level approaches the asymptotic molecular population is characterised by δ_{LZ} . To this end, we take Eqs. (99) and (100) of the two level mean field approach, where it is revealing to introduce a natural time scale $t_{\text{nat}} = (\Delta B)/(\frac{dB}{dt})$, as well as the harmonic oscillator length scale $l_{\text{ho}} = \sqrt{\hbar/(m2\pi\nu_{\text{ho}})}$. Applying these natural time and length scales to the two level mean field equations reveals that they can be characterised purely in terms of the nonlinearity parameter $k_{\text{bg}} = Na_{\text{bg}}/l_{\text{ho}}$ of the Gross-Pitaevskii equation [47], in addition to the quantities $\omega_{\text{ho}}t_{\text{nat}}$ and

$$k_{\text{eff}} = \frac{1}{\hbar} \left[\frac{dE_{\text{res}}}{dB}(B_{\text{res}}) \right] (\Delta B)^2 / (dB/dt). \quad (110)$$

Here N is the total number of atoms and $\omega_{\text{ho}} = 2\pi\nu_{\text{ho}}$ is the angular frequency of the spherically symmetric atom trap. We note that all three of these parameters can in principle be independently varied by manipulating the trap frequency, the ramp speed, and the total number of atoms. Of these three dimensionless quantities, the Landau-Zener parameter δ_{LZ} in Eq. (61) can be written as a function of just the nonlinearity parameter k_{bg} and $\omega_{\text{ho}}t_{\text{nat}}$. Indeed, as we observe in Fig. 13, keeping k_{bg} and $\omega_{\text{ho}}t_{\text{nat}}$ constant while varying k_{eff} reveals a

very weak dependence of the molecular conversion efficiency on this variation. Using identical input parameters for the dynamic equation (94) of the first order microscopic quantum dynamics approach reveals that this remarkable universality of the molecular production during a linear passage across a Feshbach resonance is preserved even when the complete quasi continuum of excited two-body energy modes is explicitly accounted for by the theory.

IV. CONCLUSIONS

We have presented a comprehensive theoretical analysis of the adiabatic association to diatomic molecules of initially Bose-Einstein condensed ^{87}Rb atoms via magnetic field tunable interactions. In particular, we have considered the situation in which a gas of Bose-Einstein condensed atoms in the ($F = 1, m_F = +1$) state is exposed to a homogeneous magnetic field whose strength is varied linearly to cross the broadest Feshbach resonance at 100 mT, in order to produce strongly correlated pairs of atoms in the highest excited vibrational bound state. We have compared the predictions of Landau-Zener, nonlinear configuration interaction, and two level mean field approaches with the full first order microscopic quantum dynamics approach, which explicitly includes all energy states of two atoms.

We found that despite decisive differences between these many-body approaches with respect to the description of the underlying microscopic binary collision dynamics, the predicted molecular production efficiencies obtained from linear ramps of the magnetic field strength are virtually independent of the level of approximation. We have shown that the Landau-Zener coefficient of Eq. (61) is the main parameter that controls the molecular production in all theoretical approaches. Consequently, the efficiency of molecular production in linear ramps of the magnetic field strength is remarkably insensitive with respect to the details of the binary collision dynamics and to the coherent nature of the gas. The adiabatic association of molecules in dilute Bose-Einstein condensed gases is thus subject to universal physical properties similar to those that we have identified in the associated two-body problem. This indicates that related experiments on the formation of molecules as well as their subsequent dissociation via linear ramps of the magnetic field strength (see, e.g., [50]) are largely inconclusive with respect to the details of the intermediate microscopic binary collision dynamics (cf., also, Ref. [54]).

The universal properties of the molecular production efficiencies and dissociation spectra reported in this paper are restricted to *linear* ramps of the magnetic field strength. The interferometric studies of Refs. [7, 8] and their subsequent theoretical analysis [45, 63, 64], for instance, have clearly revealed that sequences of linear variations of the magnetic field strength lead to molecular production efficiencies beyond the predictions of Landau-Zener or two level mean field models.

Acknowledgments

We thank Vincent Boyer, Donatella Cassetari, Rachel Godun, Eleanor Hodby, Giuseppe Smirne, C.M. Chandrashekar, Christopher Foot, Stefan Dürr, Thomas Gasenzer, and Keith Burnett for stimulating discussions. This research has been supported by the European Community Marie Curie Fellowship under Contract no. HPMF-CT-2002-02000 (K.G.), the United Kingdom Engineering and Physical Sciences Research Council as well as NASA (S.A.G.), the US Office of Naval Research (E.T. and P.S.J.), and a University Research Fellowship of the Royal Society (T.K.).

APPENDIX A: LOW ENERGY TWO CHANNEL HAMILTONIAN

In this appendix we shall provide the universal and practical model of the low energy two-channel potential matrix that we have used to determine the static as well as the dynamic properties of the resonance enhanced scattering in Sections II and III. Based on the general form of the energy states in Subsection II B, we shall determine the explicit parameters of the low energy potentials that correspond to the 100 mT Feshbach resonance of ^{87}Rb .

1. Low energy background scattering potential

The two-channel bound and continuum energy states in Subsection II B depend on the complete Green's function $G_{\text{bg}}(z)$ of the background scattering in Eq. (9). Here z is the complex parameter in Eqs. (17) and Eq. (29), respectively, which determines the asymptotic form of the continuum and bound state wave functions at large interatomic distances. The Green's function $G_{\text{bg}}(z)$ is determined by all bound and continuum energy states associated with the background scattering. The detailed form of the binary interaction potential is not resolved in ultracold collisions (cf. discussion in II B 1). At magnetic field strengths asymptotically far from the position of a Feshbach resonance, the low energy scattering observables can be determined in terms of just two parameters, the background scattering length a_{bg} and the binding energy E_{-1} (see Fig. 2) of the highest excited vibrational bound state of the background scattering potential V_{bg} [37, 69]. This universality allows us to choose a potential model of V_{bg} that recovers the exact scattering length a_{bg} as well as the exact binding energy E_{-1} . In the following, we thus use a most convenient separable potential energy operator, of the form [70]

$$V_{\text{bg}} = |\chi_{\text{bg}}\rangle \xi_{\text{bg}} \langle \chi_{\text{bg}}|, \quad (\text{A1})$$

to determine $G_{\text{bg}}(z)$. We choose the arbitrary but convenient Gaussian form of the function

$$\langle \mathbf{p} | \chi_{\text{bg}} \rangle = \chi_{\text{bg}}(p) = \frac{\exp\left(-\frac{p^2 \sigma_{\text{bg}}^2}{2\hbar^2}\right)}{(2\pi\hbar)^{3/2}} \quad (\text{A2})$$

in momentum space. We shall then adjust the amplitude ξ_{bg} and the range parameter σ_{bg} in such a way that they exactly recover a_{bg} as well as E_{-1} (see Fig. 2).

The choice of a separable potential energy operator in Eq. (A1) allows us to determine the bound state ϕ_{-1} and the continuum energy states of the background scattering in an analytic form. The bound state ϕ_{-1} and its binding energy E_{-1} are determined by the integral form of the Schrödinger equation, which for the separable potential in Eq. (A1) is given by:

$$|\phi_{-1}\rangle = G_0(E_{-1})V_{\text{bg}}|\phi_{-1}\rangle = G_0(E_{-1})|\chi_{\text{bg}}\rangle \xi_{\text{bg}} \langle \chi_{\text{bg}} | \phi_{-1} \rangle. \quad (\text{A3})$$

Here $G_0(z) = [z - (-\hbar^2 \nabla^2 / m)]^{-1}$ is the free Green's function, i.e. the Green's function of the relative motion of an atom pair in the absence of interactions. The factor $\langle \chi_{\text{bg}} | \phi_{-1} \rangle$ in Eq. (A3) is determined by the unit normalisation of ϕ_{-1} . The as yet undetermined binding energy E_{-1} can be obtained by multiplying Eq. (A3) by $\langle \chi_{\text{bg}} |$ from the left. This yields:

$$1 - \xi_{\text{bg}} \langle \chi_{\text{bg}} | G_0(E_{-1}) | \chi_{\text{bg}} \rangle = 0. \quad (\text{A4})$$

A short calculation using the Gaussian form of χ_{bg} in Eq. (A2) determines the matrix element of the free Green's function in Eq. (A4) by:

$$\langle \chi_{\text{bg}} | G_0(E_{-1}) | \chi_{\text{bg}} \rangle = \frac{m}{4\pi^{3/2}\hbar^2\sigma_{\text{bg}}} \left\{ \sqrt{\pi} x e^{x^2} [1 - \text{erf}(x)] - 1 \right\}. \quad (\text{A5})$$

Here $\text{erf}(x) = \frac{2}{\sqrt{\pi}} \int_0^x e^{-u^2} du$ is the error function with the argument $x = \sqrt{m|E_{-1}|}\sigma_{\text{bg}}/\hbar$.

In addition to Eq. (A4), the second condition that is needed to relate the two parameters ξ_{bg} and σ_{bg} of the separable potential operator to the background scattering length and the binding energy E_{-1} is provided by the continuum energy wave functions, or equivalently, by the T matrix. The T matrix of the background scattering is determined by the Lippmann-Schwinger equation [38]:

$$T_{\text{bg}}(z) = V_{\text{bg}} + V_{\text{bg}} G_0(z) T_{\text{bg}}(z). \quad (\text{A6})$$

For a separable potential energy operator Eq. (A6) can be solved by iteration, which yields the sum of the Born series:

$$T_{\text{bg}}(z) = V_{\text{bg}} \sum_{j=0}^{\infty} [G_0(z) V_{\text{bg}}]^j = \frac{|\chi_{\text{bg}}\rangle \xi_{\text{bg}} \langle \chi_{\text{bg}}|}{1 - \xi_{\text{bg}} \langle \chi_{\text{bg}} | G_0(z) | \chi_{\text{bg}} \rangle}. \quad (\text{A7})$$

The background scattering length is then determined in terms of the T matrix in Eq. (A7) by

$$a_{\text{bg}} = \frac{m}{4\pi\hbar^2} (2\pi\hbar)^3 \langle 0 | T_{\text{bg}}(0) | 0 \rangle = \frac{\frac{m}{4\pi\hbar^2} \xi_{\text{bg}}}{1 - \xi_{\text{bg}} \langle \chi_{\text{bg}} | G_0(0) | \chi_{\text{bg}} \rangle}. \quad (\text{A8})$$

Here $|0\rangle$ is the zero momentum plane wave of the relative motion of an atom pair. The denominator on the right hand side of Eq. (A8) can be obtained directly from Eq. (A5) by replacing the energy argument E_{-1} by 0. This yields:

$$a_{\text{bg}} = \frac{\frac{m}{4\pi\hbar^2} \xi_{\text{bg}}}{1 + \frac{m}{4\pi\hbar^2} \xi_{\text{bg}} / (\sqrt{\pi} \sigma_{\text{bg}})}. \quad (\text{A9})$$

Equation (A9) can be used to eliminate ξ_{bg} from Eq. (A4), which, in turn, determines the range parameter σ_{bg} in terms of the background scattering length a_{bg} and of the binding energy E_{-1} . Given the range parameter σ_{bg} the remaining amplitude ξ_{bg} can then be obtained from Eq. (A9). For the ^{87}Rb parameters $a_{\text{bg}} = 100 a_{\text{Bohr}}$ and $E_{-1} = -h \times 23 \text{ MHz}$, as obtained from Fig. 1, this yields $\sigma_{\text{bg}} = 42.90753599 a_{\text{Bohr}}$ and $m\xi_{\text{bg}}/(4\pi\hbar^2) = -317.5649079 a_{\text{Bohr}}$.

2. Off diagonal coupling

In order to recover the universal properties of the near resonant bound states in Subsection II C (cf. Fig. 4), the transition probabilities in Subsection II D (cf. Fig. 5), as well as the time evolution operator in Eq. (94), it is sufficient to use a single channel Hamiltonian, as explained in Subsection II C. To this end, we have extended the potential model in Eq. (A1) to recover not only the background scattering, but also the scattering length $a(B)$. We have thus adjusted the separable potential energy operator in Eq. (A1), at each magnetic field strength B , to the magnetic field dependent scattering length $a(B) = a_{\text{bg}} [1 - (\Delta B)/(B - B_0)]$ and to the energy E_{-1} (cf., also, Ref. [45]).

The dissociation spectra in Subsection II F have been obtained from a two channel description. A two channel approach recovers not only the exact magnetic field dependence of the scattering length, but it also accurately describes the binding energies of the multichannel bound states over a much wider range of magnetic field strengths (see Fig. 2) than a single channel treatment. Apart from the background scattering, a two channel description of resonance enhanced collisions requires us to specify the coupling between the open and the closed channels. Equations (25) and (26) relate the off diagonal coupling element $W(r)$ of the general two channel Hamiltonian in Eq. (2) to the resonance width (ΔB) as well as to the shift $B_0 - B_{\text{res}}$. Although the resonance shift is not directly measurable, Eq. (32) relates it to the van der Waals dispersion coefficient C_6 and to the width (ΔB) , which can usually be determined from experimental data. In the pole approximation to the closed channel Green's function [cf. Eq. (15)], the closed channel part of the two channel Hamiltonian in Eq. (2) reduces to Eq. (20), which restricts the state of an atom pair in the closed channels to the resonance state ϕ_{res} . Given the linear dependence of the energy $E_{\text{res}}(B)$, associated with ϕ_{res} , on the magnetic field strength B , the closed channel part of the two channel Hamiltonian is determined completely by the slope $\left[\frac{dE_{\text{res}}}{dB}(B_{\text{res}})\right]$ of the Feshbach resonance (cf. Subsection II B).

The only remaining quantity that needs to be determined is the product $W(r)\phi_{\text{res}}(r)$, which provides the interchannel coupling in the pole approximation. Similar to the choice of the separable potential in Eq. (A1), we shall use a two parameter description of the interchannel coupling, in terms of a real amplitude ζ and a range parameter σ , to recover the width and the shift of the Feshbach resonance. This leads to the *ansatz*

$$W|\phi_{\text{res}}\rangle = |\chi\rangle\zeta, \quad (\text{A10})$$

where we have chosen the arbitrary but convenient Gaussian form of the function

$$\langle \mathbf{p}|\chi\rangle = \chi(p) = \frac{\exp\left(-\frac{p^2\sigma^2}{2\hbar^2}\right)}{(2\pi\hbar)^{3/2}} \quad (\text{A11})$$

in momentum space. In the following, we shall adjust the parameters ζ and σ in such a way that the two channel Hamiltonian recovers the resonance width (ΔB) and the shift $B_0 - B_{\text{res}}$ via Eqs. (25) and (26), respectively. To this end, we shall first determine the zero energy continuum state $\phi_0^{(+)}$ in Eq. (25) and the zero energy Green's function $G_{\text{bg}}(0)$ in Eq. (26) in terms of the T matrix associated with the background scattering, which is given by Eq. (A6). The continuum energy states associated with the relative momentum \mathbf{p} fulfil the Lippmann-Schwinger equation [38] ($E = p^2/m$):

$$|\phi_{\mathbf{p}}^{(+)}\rangle = |\mathbf{p}\rangle + G_0(E + i0)T_{\text{bg}}(E + i0)|\mathbf{p}\rangle. \quad (\text{A12})$$

Here the energy argument “ $z = E + i0$ ” ensures that the wave function $\phi_{\mathbf{p}}^{(+)}(\mathbf{r})$ has the long range asymptotic form of Eq. (8). Furthermore, the Green's function $G_{\text{bg}}(z)$ is completely determined by the T matrix in Eq. (A6) in terms of the general formula [38]:

$$G_{\text{bg}}(z) = G_0(z) + G_0(z)T_{\text{bg}}(z)G_0(z). \quad (\text{A13})$$

In the separable potential approach the exact T matrix of the background scattering is given by Eq. (A7), so that the subsequent determination of the right hand sides of Eqs. (25) and (26) involves just the evaluation of matrix elements of the zero energy free Green's function $G_0(0)$ between the wave functions χ_{bg} and χ . Given the Gaussian form of these wave functions in Eqs. (A2) and (A11), the matrix elements can be readily determined analytically in complete analogy to Eq. (A5). This yields

$$(\Delta B) = \frac{\zeta^2}{\left[\frac{dE_{\text{res}}}{dB}(B_{\text{res}})\right]} \frac{m}{4\pi\hbar^2 a_{\text{bg}}} \left(1 - \frac{a_{\text{bg}}}{\sqrt{\pi}\bar{\sigma}}\right)^2 \quad (\text{A14})$$

for the resonance width and

$$B_0 - B_{\text{res}} = (\Delta B) \frac{a_{\text{bg}}}{\sqrt{\pi}\sigma} \frac{1 - \frac{a_{\text{bg}}}{\sqrt{\pi}\sigma} \left(\frac{\sigma}{\bar{\sigma}}\right)^2}{\left(1 - \frac{a_{\text{bg}}}{\sqrt{\pi}\sigma} \frac{\sigma}{\bar{\sigma}}\right)^2} \quad (\text{A15})$$

for the shift. Here we have introduced the mean range parameter

$$\bar{\sigma} = \sqrt{\frac{1}{2}(\sigma^2 + \sigma_{\text{bg}}^2)}. \quad (\text{A16})$$

Inserting the experimentally known width of the resonance and Eq. (32) for the shift into the left hand side of Eqs. (A14) and (A15), respectively, then determines ζ and σ in terms of (ΔB) , C_6 and the slope of the resonance. Using $(\Delta B) = 0.02 \text{ mT}$ [44], $C_6 = 4660 \text{ a.u.}$ [42] and $\left[\frac{dE_{\text{res}}}{dB}(B_{\text{res}})\right] = h \times 38 \text{ MHz/mT}$ for the 100 mT Feshbach resonance of ^{87}Rb , the parameters of the interchannel coupling can be summarised as $\sigma = 21.50035463 a_{\text{Bohr}}$ and $m\zeta^2/(4\pi\hbar^2\sigma) = h \times 8.0536126 \text{ MHz}$.

-
- [1] For a review see: B. Goss Levi, *Physics Today* **53**, no. 9, 46 (2000).
- [2] J. Weiner, V. Bagnato, S. Zilio, and P.S. Julienne, *Rev. Mod. Phys.* **71**, 1 (1999).
- [3] M. Randeria, in: *Bose-Einstein condensation*, edited by A. Griffin, D.W. Snoke, and S. Stringari, 355 (Cambridge University Press, Cambridge, 1995).
- [4] M. Baranov, Ł. Dobrek, K. Góral, L. Santos, and M. Lewenstein, *Phys. Scr.* **T102**, 74 (2002).
- [5] R. Wynar, R.S. Freeland, D.J. Han, C. Ryu, and D.J. Heinzen, *Science* **287**, 1016 (2000).
- [6] S. Inouye, M.R. Andrews, J. Stenger, H.-J. Miesner, D.M. Stamper-Kurn, and W. Ketterle, *Nature (London)* **392**, 151 (1998).
- [7] E.A. Donley, N.R. Claussen, S.T. Thompson, and C.E. Wieman, *Nature (London)* **417**, 529 (2002).
- [8] N.R. Claussen, S.J.J.M.F. Kokkelmans, S.T. Thompson, E.A. Donley, E. Hodby, and C.E. Wieman, *Phys. Rev. A* **67**, 060701 (2003).
- [9] J. Herbig, T. Kraemer, M. Mark, T. Weber, C. Chin, H.-Ch. Nägerl, and R. Grimm, *Science* **301**, 1510 (2003).
- [10] S. Dürr, T. Volz, A. Marte, and G. Rempe, *Phys. Rev. Lett.* **92**, 020406 (2004).
- [11] K. Xu, T. Mukaiyama, J.R. Abo-Shaer, J.K. Chin, D.E. Miller, and W. Ketterle, *Phys. Rev. Lett.* **91**, 210402 (2003).
- [12] C.A. Regal, C. Ticknor, J.L. Bohn, and D.S. Jin, *Nature (London)* **424**, 47 (2003).
- [13] K.E. Strecker, G.B. Partridge, and R.G. Hulet, *Phys. Rev. Lett.* **91**, 080406 (2003).
- [14] J. Cubizolles, T. Bourdel, S.J.J.M.F. Kokkelmans, G.V. Shlyapnikov, and C. Salomon, *Phys. Rev. Lett.* **91**, 240401 (2003).
- [15] S. Jochim, M. Bartenstein, A. Altmeyer, G. Hendl, C. Chin, J. Hecker Denschlag, and R. Grimm, *Phys. Rev. Lett.* **91**, 240402 (2003).
- [16] C. A. Regal, M. Greiner, and D. S. Jin, *Phys. Rev. Lett.* **92**, 083201 (2004).
- [17] M. Greiner, C.A. Regal, and D.S. Jin, *Nature (London)* **426**, 537 (2003).
- [18] S. Jochim, M. Bartenstein, A. Altmeyer, G. Hendl, S. Riedl, C. Chin, J. Hecker Denschlag, and R. Grimm, *Science* **302**, 2101 (2003).
- [19] M.W. Zwierlein, C.A. Stan, C.H. Schunck, S.M.F. Raupach, S. Gupta, Z. Hadzibabic, and W. Ketterle, *Phys. Rev. Lett.* **91**, 250401 (2003).
- [20] M. Bartenstein, A. Altmeyer, S. Riedl, S. Jochim, C. Chin, J. Hecker Denschlag, and R. Grimm, *Phys. Rev. Lett.* **92**, 120401 (2004).
- [21] C. A. Regal, M. Greiner, and D. S. Jin, *Phys. Rev. Lett.* **92**, 040403 (2004).
- [22] M. W. Zwierlein, C. A. Stan, C. H. Schunck, S. M. F. Raupach, A. J. Kerman, and W. Ketterle, *Phys. Rev. Lett.* **92**, 120403 (2004).
- [23] M. Bartenstein, A. Altmeyer, S. Riedl, S. Jochim, C. Chin, J. Hecker Denschlag, and R. Grimm, *arXiv.org eprint cond-mat/0403716* (2004).
- [24] P. Soldán, M.T. Cvitaš, J.M. Hutson, P. Honvault and J.-M. Launay, *Phys. Rev. Lett.* **89**, 153201 (2002).
- [25] A. Marte, T. Volz, J. Schuster, S. Dürr, G. Rempe, E.G.M. van Kempen, and B.J. Verhaar, *Phys. Rev. Lett.* **89**, 283202 (2002).
- [26] T. Köhler and K. Burnett, *Phys. Rev. A* **65**, 033601 (2002).
- [27] P.D. Drummond, K.V. Kheruntsyan, and H. He, *Phys. Rev. Lett.* **81**, 3055 (1998).
- [28] E. Timmermans, P. Tommasini, M. Hussein, and A. Kerman, *Phys. Rep.* **315**, 199 (1999).
- [29] V.A. Yurovsky, A. Ben-Reuven, P.S. Julienne, and C.J. Williams, *Phys. Rev. A* **62**, 043605 (2000).
- [30] K. Góral, M. Gajda, and K. Rzążewski, *Phys. Rev. Lett.* **86**, 1397 (2001).
- [31] A.N. Salgueiro, M.C. Nemes, M.D. Sampaio, and A.F.R.D. Piza, *Physica A* **290**, 4 (2001).
- [32] S.K. Adhikari, *J. Phys. B* **34**, 4231 (2001).
- [33] B.J. Cusack, T.J. Alexander, E.A. Ostrovskaya, and Y.S. Kivshar, *Phys. Rev. A* **65**, 013609 (2002).
- [34] F.K. Abdullaev and V.V. Konotop, *Phys. Rev. A* **68**, 013605 (2003).
- [35] P. Naidon and F. Masnou-Seeuws, *Phys. Rev. A* **68**, 033612 (2003).
- [36] F.H. Mies, E. Tiesinga, and P.S. Julienne, *Phys. Rev. A* **61**, 022721 (2000).
- [37] B. Gao, *Phys. Rev. A* **58**, 4222 (1998).
- [38] R.G. Newton, *Scattering Theory of Waves and Particles* (Springer, New York, 1982).
- [39] M.S. Child, *Molecular Collision Theory* (Academic, London, 1974).
- [40] The derivation of the formula is based on ideas of multichannel quantum defect theory as outlined in: P.S. Julienne and F.H. Mies, *J. Opt. Soc. Am. B* **6**, 2257 (1989).
- [41] G.F. Gribakin and V.V. Flambaum, *Phys. Rev. A* **48**, 546 (1993).
- [42] J.L. Roberts, J.P. Burke, Jr., N.R. Claussen, S.L. Cornish, E.A. Donley, and C.E. Wieman, *Phys. Rev. A* **64**, 024702 (2001).
- [43] E.G.M. van Kempen, S.J.J.M.F. Kokkelmans, D.J. Heinzen, and B.J. Verhaar, *Phys. Rev. Lett.* **88**, 093201 (2002).
- [44] T. Volz, S. Dürr, S. Ernst, A. Marte, and G. Rempe, *Phys. Rev. A* **68**, 010702 (2003).
- [45] T. Köhler, T. Gasenzer, and K. Burnett, *Phys. Rev. A* **67**, 013601 (2003).
- [46] We note that the ^{87}Rb atoms in the ($F = 1, m_F = +1$) electronic ground state cannot be magnetically trapped. The harmonic potential is, therefore, provided by crossed laser beams. These optical atom traps can confine atoms and molecules at the same time.
- [47] F. Dalfovo, S. Giorgini, L.P. Pitaevskii, and S. Stringari, *Rev. Mod. Phys.* **71**, 463 (1999).
- [48] A.L. Fetter and D.L. Feder, *Phys. Rev. A* **58**, 3185 (1998).
- [49] Yu.N. Demkov and V.I. Osherov, *Sov. Phys. JETP* **26**, 916 (1968).
- [50] This formula for the spectral density can also be obtained from the intuitive derivation of: T. Mukaiyama, J.R. Abo-Schaer, K. Xu, J.K. Chin, and W. Ketterle, e-print *arXiv cond-mat/0311558*.
- [51] S.L. Cornish, N.R. Claussen, J.L. Roberts, E.A. Cornell, and C.E. Wieman, *Phys. Rev. Lett.* **85**, 1795 (2000).
- [52] T. Köhler, *Phys. Rev. Lett.* **89**, 210404 (2002).
- [53] T. Köhler, T. Gasenzer, P.S. Julienne, and K. Burnett, *Phys. Rev. Lett.* **91**, 230401 (2003).
- [54] T. Köhler, K. Góral, and T. Gasenzer, e-print *arXiv cond-mat/0305060*.
- [55] J. Fricke, *Ann. Phys. (N.Y.)* **252**, 479 (1996).
- [56] A.L. Fetter and J.D. Walecka, *Quantum Theory of Many-Particle Systems* (McGraw-Hill, New York, 1971).
- [57] For a general description of the detection of composite particles

- see, e.g., J.D. Dollard, J. Math. Phys. **14**, 708 (1973).
- [58] The second, factorised contribution to the molecular mean field on the right hand side of Eq. (88) can be interpreted as an overlap between the atomic mean field and the molecular bound state wave function. When the gas is strongly interacting the molecular bound state has a spatial extent comparable to the mean distance of the atoms in the gas (cf. Eq. (41)), and the overlap becomes significant. As a consequence, one and the same atom could contribute to several bound molecules, so that a separation of the gas into bound and free atoms becomes physically meaningless.
- [59] Private communication from V. Boyer, D. Cassetari, R.M. Godun, G. Smirne, C.M. Chandrashekar, and C.J. Foot.
- [60] An explicit determination of the energy spectra of the burst atoms and their typical single particle energy scale of $k_B \times 150$ nK in the atom-molecule coherence experiments of Ref. [7] has been performed in Ref. [45].
- [61] F.A. van Abeelen and B.J. Verhaar, Phys. Rev. Lett. **83**, 1550 (1999). This work also accounts for the finite lifetime of the closed channel resonance state in terms of a decay constant.
- [62] The admixture of the resonance state to the highest excited vibrational bound state depends on the Feshbach resonance. Over the whole range of magnetic field strengths between 15.5 mT and 16.22 mT in the atom-molecule coherence experiments [7] with ^{85}Rb Bose-Einstein condensates, the admixture of the resonance state is even less than 30 % (cf., also, Ref. [53]).
- [63] S.J.J.M.F. Kokkelmans and M.J. Holland, Phys. Rev. Lett. **89**, 180401 (2002).
- [64] M. Mackie, K.-A. Suominen, and J. Javanainen, Phys. Rev. Lett. **89**, 180403 (2002).
- [65] V.A. Yurovsky and A. Ben-Reuven, Phys. Rev. A **67**, 043611 (2003).
- [66] B. Borca, D. Blume, and C.H. Greene, New J. Phys. **5**, 111 (2003).
- [67] E. Braaten, H.-W. Hammer, and M. Kusunoki, e-print cond-mat/0301489.
- [68] R.A. Duine and H.T.C. Stoof, Phys. Rev. A **68**, 013602 (2003).
- [69] An equivalent choice of parameters would be a_{bg} and the van der Waals dispersion coefficient C_6 [37].
- [70] C. Lovelace, Phys. Rev. **135**, B1225 (1964).